Electronic Supplementary Material (ESI) for Dalton Transactions.

Electronic supplementary information

Imidazolyl-pyreno-imidazole conjugate as cyanide sensor and set-reset memorized sequential logic device

Sourav Mardanya, Srikanta Karmakar, Debiprasad Mondal and Sujoy Baitalik*

Department of Chemistry, Inorganic Chemistry Section, Jadavpur University, Kolkata – 700032, India

Physical measurements

Elemental analyses of the compounds were performed with a Vario-Micro V2.0.11 elemental (CHNSO) analyzer. NMR spectra were collected on a Bruker 300 spectrometer in DMSO-d_6, and high resolution mass spectroscopy was performed on a Waters Xevo G2 QTOf mass spectrometer. The UV/vis absorption spectra were recorded with a Shimadzu UV 1800 spectrometer. A matched pair of quartz cuvettes (path length 1 cm) was employed. Steady state luminescence spectra were obtained either by a Perkin–Elmer LS55 or Spex fluorolog-2 spectrofluorometer equipped with DM3000F software. All the UV-vis absorption and emission measurements were carried out at room temperature. Luminescence quantum yields were determined by using literature method taking quinine sulphate as the standard. Luminescence lifetime measurements were carried out by using time–correlated single photon counting set up from Horiba Jobin-Yvon. The luminescence decay data were collected on a Hamamatsu MCP photomultiplier (R3809) and were analyzed by using IBH DAS6 software.

Experimental uncertainties are as follows: absorption maxima, ±2 nm; molar absorption coefficients, 10%; emission maxima, ±5 nm; excited–state lifetimes, 10%; luminescence quantum yields, 20%.

Anion sensing experiments

For a typical absorption and emission titration experiment, aliquots of a TBA salts of F^-, Cl^-, Br^-, I^-, CN^-, NO_3^-, CH_3COO^-, $H_2PO_4^-$, ClO_4^-, and OH^- (2.0×10^{-2} M) and perchlorate salts of metal ions (5×10^{-3} M) were added incrementally to a 2.5 mL solution of the receptor (2.0×10^{-5} M). The equilibrium constants were evaluated from the absorbance data using equation 'S1'.[S1]

$$A_{\mathrm{obs}} = (A_0 + A_\infty K[\mathrm{G}]_\mathrm{T})/(1 + K[\mathrm{G}]_\mathrm{T}) \qquad \text{(S1)}$$

where A_{obs} is the observed absorbance, A_0 is the absorbance of the free receptor, A_∞ is the maximum absorbance induced by the presence of a given anionic guest, $[\mathrm{G}]_\mathrm{T}$ is the total concentration of the guest, and K is the equilibrium constant of the host–guest entity. Binding constants were performed in duplicate, and the average value is reported. The lifetimes of the receptors were recorded as a function of different anions and solvents.

X-ray crystallographic analyses

The crystallographic data, details of data collection, and refinement parameter for the receptor Py-BiimzH$_2$ were summarized in Table S1. In each case, single crystals of suitable size were obtained by diffusing toluene to 1:1 acetonitrile-dichlorometane solution of the complexes. The crystals were immersed in paratone oil and then mounted on the tip of a glass fiber and cemented using epoxy resin. Intensity data for these crystals were collected using MoKα (λ = 0.7107 Å) radiation on a Bruker SMART APEX II diffractometer equipped with CCD area detector at room temperature. The data integration and reduction were processed with SAINT[S2] software provided with the software package of SMART APEX II. An empirical absorption correction was applied to the collected reflections with SADABS.[S2] The structures were solved by direct methods using SHELXTL[S3] and were refined on F^2 by the full-matrix least-squares technique using the SHELXL-97 program package.[S4] Graphics were generated using PLATON.[S5] In both cases, the non-hydrogen atoms were refined anisotropically until the convergence. All the hydrogen atoms were geometrically positioned and treated as riding atoms.

CCDC reference number for Py-BiimzH$_2$ is 1040155.

Theoretical computational methods

All calculations were performed with the Gaussian 09 program[S6] package employing the DFT method with Becke's three-parameter hybrid functional and Lee-Yang-Parr's gradient corrected correlation functional (B3LYP) level of theory using 6-31g(d) basis set for the ligands (Py-BiimzH$_2$, Py-BiimzH and Py-Biimz). For the metal complex LanL2DZ basis set is used.[S7- S8] Geometries were fully optimized using the criteria of the respective programs. To compute the UV-vis transitions of the compounds, the singlet excited state geometries corresponding to the vertical excitations were optimized using the time-dependent DFT (TD-DFT) scheme starting with the ground state geometries optimized in solution phase.[S9- S10] The excitation energies, computed in DMSO were simulated by PCM model.[S11- S12] The geometries of the lowest energy singlet states of the compounds were also optimized in DMSO by using TD-DFT method and employing the PCM models to calculate the emission energies. Orbital and fractional contribution analysis was done with Gauss View[S13] and Gauss Sum 2.1.[S14]

Table S1 Crystallographic data for Py-BiimzH_2

Compound	**Py-BiimzH$_2$**
Formula	C20 H12 N4
fw	308.34
T (K)	273(2)
Cryst. Syst.	orthorhombic
Space group	Pbca
a (Å)	9.5539(7)
b (Å)	20.0561(15)
c (Å)	15.3565(11)
α (deg)	90.00
β (deg)	90.00
γ (deg)	90.00
V (Å^3)	2942.5(4)
Dc(g cm^{-3})	1.392
Z	8
μ (mm^{-1})	0.086
F(000)	1280.0
θ range (deg)	2.03-26.00
Data/restraints/params	2891/0/218
GOF on F^2	0.981
R_1 [$I > 2\sigma(I)$]^a,	0.0672
wR_2 (all data)^b	0.1874
$\Delta\rho_{max}/\Delta\rho_{min}$ (e Å)	0.045/ -0.320

^{a}R1(F) = [$\sum \| F_0 | - |F_C \| / \sum | F_0$], ^{b}wR2 (F^2) = [$\sum w(F_0^2 - F_C^2)^2 / \sum w(F_0^2)^2]^{1/2}$

Table S2 All bond distances (Å) for Py-BiimzH$_2$

Py-BiimzH$_2$			
N3-C4	1.319(4)	C7-C8	1.389(5)
N3-C6	1.367(4)	C7-C6	1.440(4)
N3-H3N	0.86	C6-C5	1.373(4)
N1-C3	1.322(4)	C4-C3	1.441(5)
N1-C1	1.375(4)	C1-C2	1.343(5)
N2-C3	1.348(4)	C5-C18	1.430(4)
N2-C2	1.367(4)	C18-C17	1.393(4)
N2-H2N	0.86	C18-C19	1.426(4)
N4-C4	1.371(4)	C19-C14	1.425(5)
N4-C5	1.395(4)	C8-C9	1.383(5)
C10-C9	1.378(6)	C12-C13	1.336(6)
C10-C11	1.390(6)	C13-C14	1.442(5)
C11-C20	1.414(5)	C14-C15	1.384(5)
C11-C12	1.438(6)	C15-C16	1.378(5)
C20-C7	1.419(5)	C16-C17	1.379(5)
C20-C19	1.438(5)		

Table S3 All bond angles (deg) for Py-BiimzH$_2$

Py-BiimzH$_2$					
C4-N4-C5	105.5(3)	N4-C5-C18	130.0(3)	C5-C6-C7	121.7(3)
C3-N1-C1	104.4(3)	N3-C4-N4	112.4(3)	C16-C17-C18	120.1(4)
C4-N3-C6	105.6(3)	N3-C4-C3	123.8(3)	C11-C20-C7	118.8(4)
C4-N3-H3N	127.2	N4-C4-C3	123.3(3)	C11-C20-C19	119.8(4)
C6-N3-H3N	127.2	N1-C3-N2	111.7(3)	C7-C20-C19	121.3(3)
C15-C14-C19	119.4(4)	N1-C3-C4	126.2(3)	C3-N2-C2	107.0(3)
C15-C14-C13	122.5(4)	N2-C3-C4	121.6(3)	C3-N2-H2N	126.5
C19-C14-C13	118.1(4)	C10-C11-C20	119.2(4)	C2-N2-H2N	126.5
C14-C19-C18	118.3(3)	C10-C11-C12	122.2(4)	C16-C15-C14	121.2(4)
C14-C19-C20	119.9(3)	C20-C11-C12	118.6(4)	C2-C1-N1	110.9(3)
C18-C19-C20	121.7(3)	C9-C10-C11	121.5(4)	C13-C12-C11	121.8(4)
C17-C18-C19	120.1(3)	C8-C7-C20	120.0(3)	C10-C9-C8	120.0(4)
C17-C18-C5	124.7(3)	C8-C7-C6	123.7(3)	C9-C8-C7	120.5(4)
C19-C18-C5	115.1(3)	C20-C7-C6	116.2(3)	C15-C16-C17	120.8(4)
C6-C5-N4	106.0(3)	N3-C6-C5	110.4(3)	C12-C13-C14	121.7(4)
C6-C5-C18	123.8(3))	N3-C6-C7	127.8(3)	C1-C2-N2	105.9(3)

Table S4 Occurrence of H-bonding interactions in Py-BiimzH_2

Compound	Atoms Label	Distance / Å
Py-BiimzH_2	H2N-------N1	2.266
	H3N-------N4	2.159

Table S5 Occurrence of π---- π and CH--- π interactions in Py-BiimzH_2

Compound	Centroid……….Centroid/H Labels	Distance / Å
Py-BiimzH_2	C16 C17 C15 C14 C19 C18-------C7 C6 C5 C18 C19 C20	3.698
	C18 C19 C20 C7 C6 C5-------C19 C18 C17 C16 C15 C14	3.698
	H1-------C11 C20 C7 C8 C9 C10	2.732
	H2-------C12C13C14C19C20C11	2.885

Table S6 Spectrophotometric and fluorimetric detection limit of Py-BiimzH_2 (2.0×10^{-5} M) in DMSO and H_2O-DMSO (9:1 v/v) solution at 298 K

Detection Limit		
Anion	**In DMSO Solution**	
	Absorption	Emission
F^-	1.77×10^{-7}	1.54×10^{-7}
CN^-	1.98×10^{-7}	1.70×10^{-7}
Anion	**In H_2O-DMSO (9:1 v/v) solution**	
	Absorption	Emission
CN^-	1.10×10^{-6}	1.04×10^{-6}

Table S7 Selected MOs along with their energies and compositions in the ground state for Py-BiimzH$_2$, Py-BiimzH and Py-Biimz in DMSO

Py-BiimzH$_2$				**Py-BiimzH**			**Py-Biimz**		
	(%) Composition			(%) Composition			(%) Composition		
MO	Energy / eV	Pyrene imidazol	Imidazol	Energy / eV	Pyrene imidazol	Imidazol	Energy/ eV	Pyrene imidazol	Imidazol
LUMO+3	0.12	97.83	2.16	-0.10	99.68	0.32	0.29	97.90	2.10
LUMO+2	-0.61	83.20	16.80	-0.48	91.99	8.01	0.13	96.33	3.67
LUMO+1	-1.08	76.35	23.64	-1.06	98.13	1.87	-0.70	98.66	1.34
LUMO	-1.55	97.20	2.79	-1.69	99.63	0.37	-1.32	99.85	0.15
HOMO	-5.26	84.02	15.97	-4.87	53.71	46..29	-4.20	63.72	36.28
HOMO-1	-6.15	67.64	32.35	-5.83	72.45	27.55	-5.40	65.35	34.65
HOMO-2	-6.33	89.03	10.96	-6.35	96.26	3.73	-5.57	98.17	1.83
HOMO-3	-7.11	73.44	26.55	-6.64	6.89	93.11	-6.02	42.66	57.34

Table S8 Selected MOs along with their energies and compositions in the singlet excited state for Py-BiimzH$_2$, Py-BiimzH and Py-Biimz in DMSO

Py-BiimzH$_2$				**Py-BiimzH**			**Py-Biimz**		
	(%) Composition			(%) Composition			(%) Composition		
MO	Energy / eV	Pyrene imidazol	Imidazol	Energy / eV	Pyrene imidazol	Imidazol	Energy/ eV	Pyrene imidazol	Imidazol
LUMO+3	0.12	98.38	1.62	0.39	98.05	1.95	0.90	99.94	0.06
LUMO+2	-0.61	83.51	16.49	0.05	88.73	11.27	0.82	87.81	12.19
LUMO+1	-1.08	78.60	21.40	-0.69	97.94	2.06	-0.23	98.39	1.61
LUMO	-1.55	97.72	2.28	-1.35	99.73	0.27	-0.89	99.98	0.02
HOMO	-5.26	85.17	14.83	-4.40	48.44	51.56	-3.59	52.89	47.11
HOMO-1	-6.15	68.70	31.30	-5.47	75.87	24.13	-4.91	62.34	37.65
HOMO-2	-6.33	89.52	10.48	-6.02	77.56	22.44	-5.07	95.99	4.01
HOMO-3	-7.11	73.92	26.08	-6.11	60.43	39.57	-5.33	22.00	88.00

Table S9 Selected MOs along with their energies and compositions of $[Cu(Py\text{-}BiimzH_2)_2]^{2+}$ for ground state α and β MOs in DMSO

$[Cu(Py\text{-}BiimzH_2)_2]^{2+}$ (α MO)					**$[Cu(Py\text{-}BiimzH_2)_2]^{2+}$** (β MO)			
	(%) Composition				(%) Composition			
MO	Energy/ eV	Pyrene imidazol	Imidazol	Cu	Energy/ eV	Pyrene imidazol	Imidazol	Cu
LUMO+3	-2.08	98.87	0.96	0.16	-2.18	98.65	0.35	0.99
LUMO+2	-2.18	99.03	0.14	0.82	-2.52	57.83	41.57	0.59
LUMO+1	-2.55	57.33	42.11	0.55	-2.65	53.29	42.39	4.31
LUMO	-2.71	53.26	43.11	3.62	-4.67	15.83	20.10	64.56
HOMO	-6.00	94.16	5.78	0.05	-5.99	94.08	5.85	0.06
HOMO-1	-6.00	93.95	6.01	0.02	-6.0	93.89	6.08	0.03
HOMO-2	-6.86	99.20	0.71	0.08	-6.85	99.01	0.86	0.12
HOMO-3	-6.90	99.07	0.82	0.09	-6.90	98.76	1.07	0.17

Table S10 Fluorescence emission of $Py\text{-}BiimzH_2$, Py-BiimzH and Py-Biimz in DMSO according to TD-DFT calculations and associated experimental value

Compound	Transition (C.I)	Energy /eV	λ_{cal}/nm	λ_{expt}/nm
$Py\text{-}BiimzH_2$	L→H(97%)(0.696)	2.93	423	423
Py-BiimzH	L→H(99%)(0.703)	2.33	532	510
Py-Biimz	L→H(99%)(0.70399)	1.92	645	510

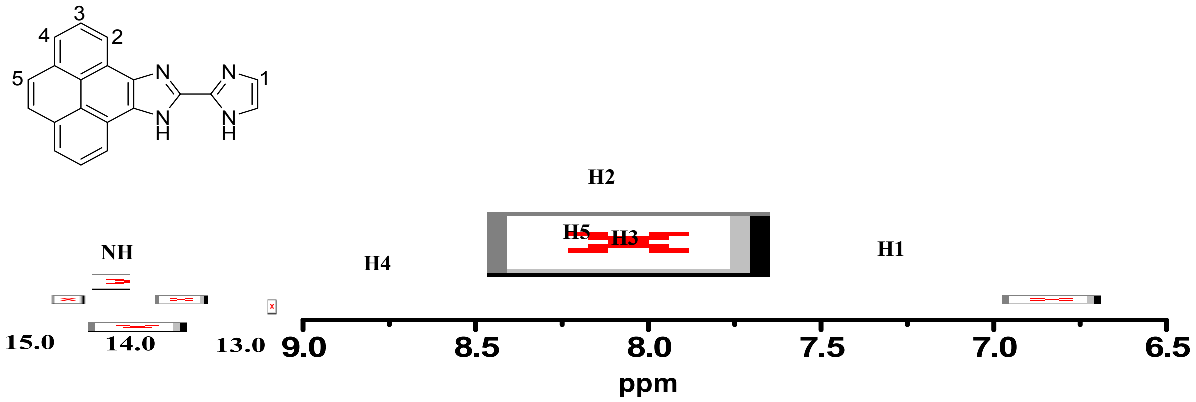

Fig. S1 ^{1}H NMR (300 MHz) spectrum of Py-BiimzH$_2$ (1.5 × 10^{-4} M) in DMSO-d_6.

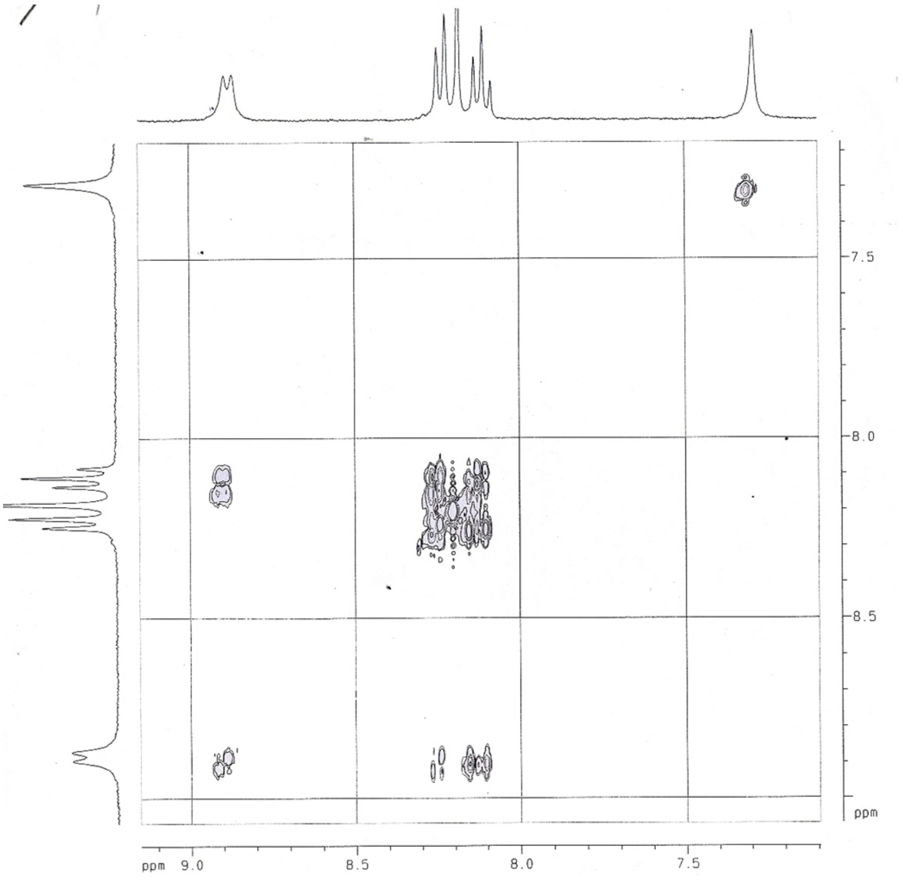

Fig. S2 ^{1}H-^{1}H COSY NMR spectrum of Py-BiimzH$_2$ in DMSO-d_6

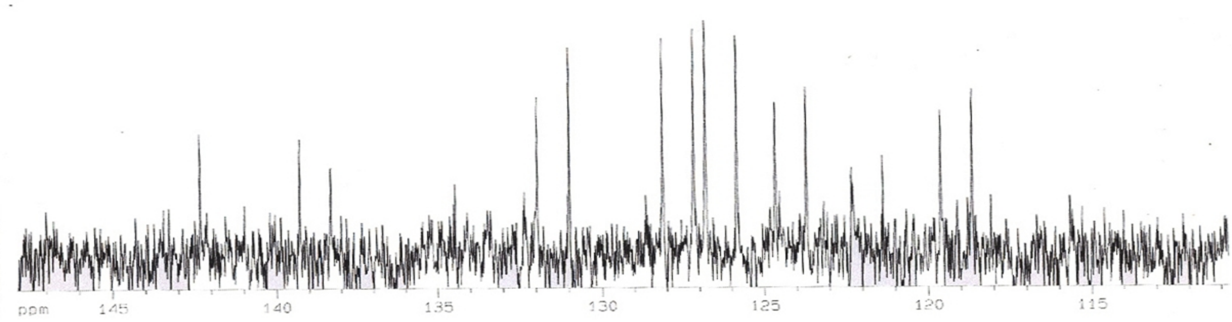

Fig. S3 ^{13}C NMR spectrum of Py-BiimzH$_2$ in DMSO-d_6.

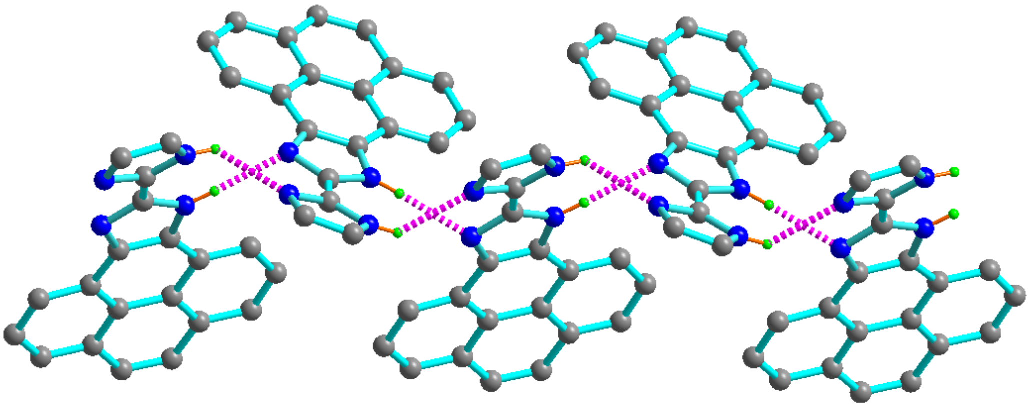

Fig. S4 Strong H-bonding interactions within the molecule.

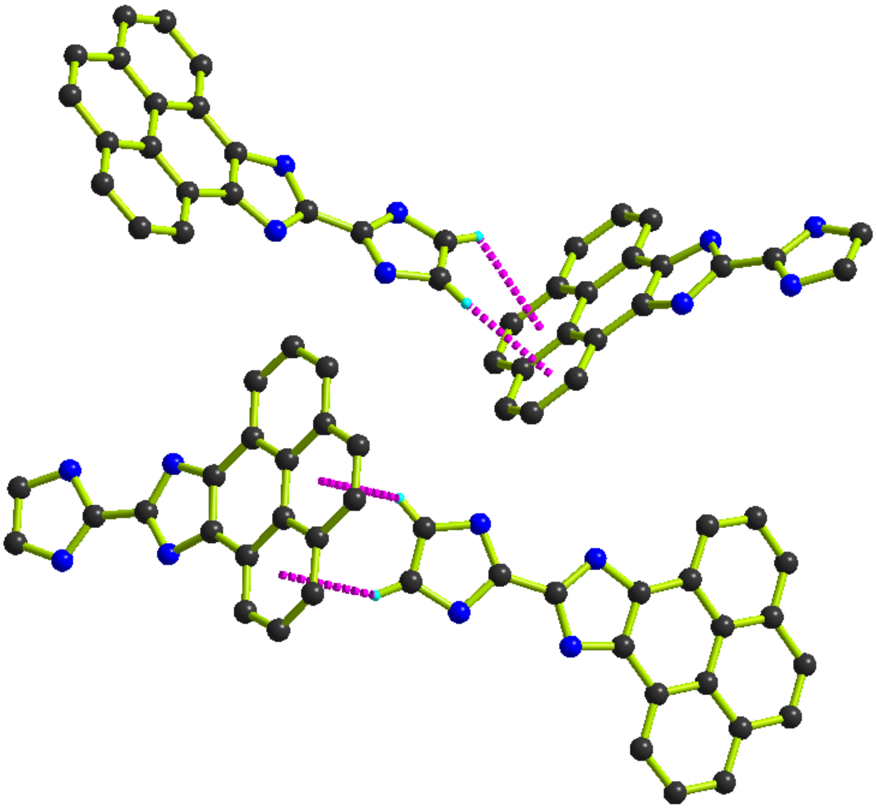

Fig. S5 Occurrence of CH–π interactions within the molecule.

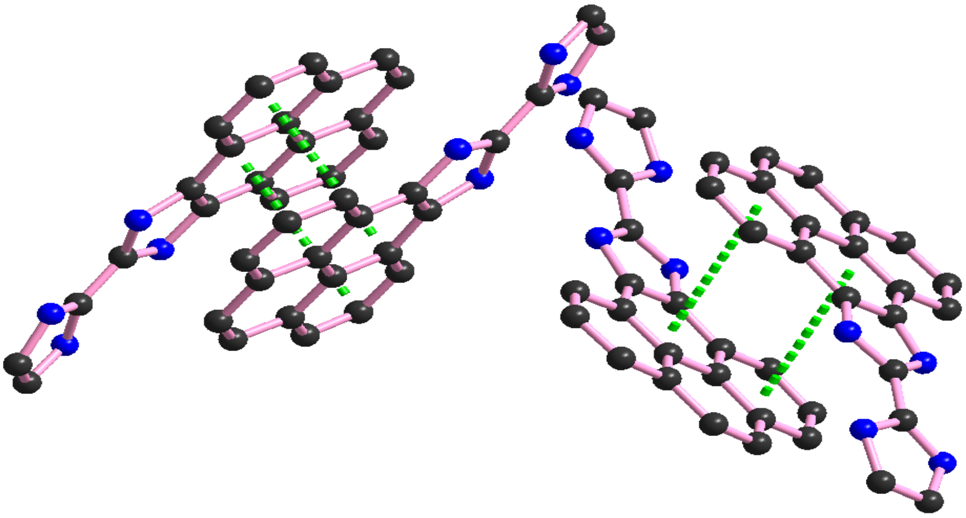

Fig. S6 Occurrence of strong π –π interactions within the molecule.

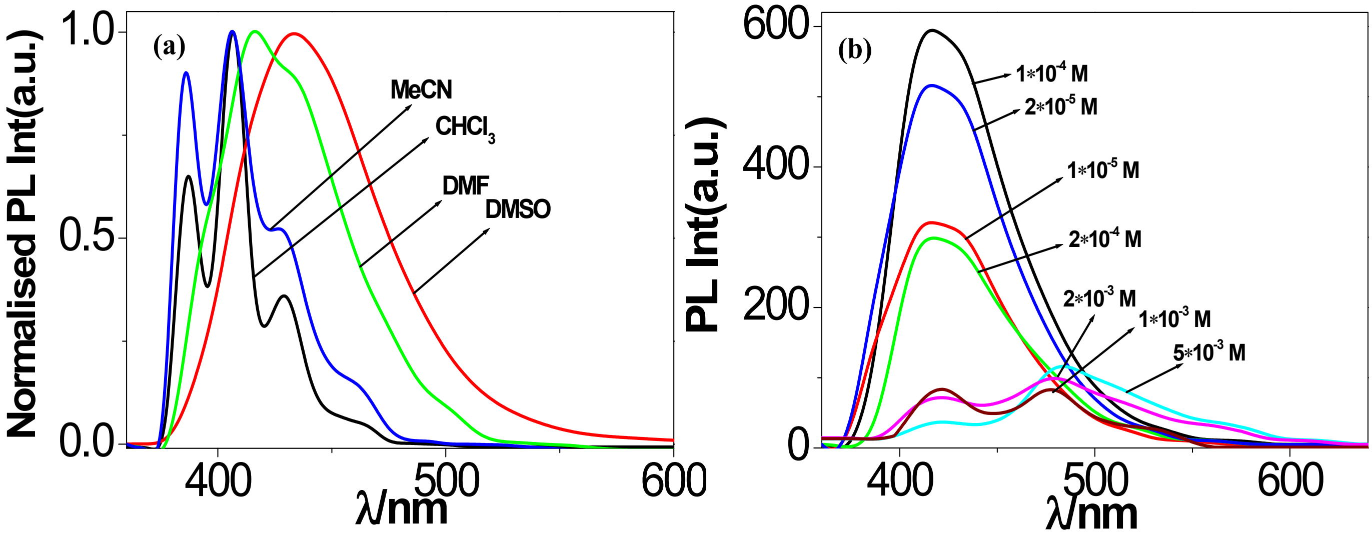

Fig. S7 Normalised emission spectra of Py-BiimzH_2 (2.0×10^{-5} M) in few selective solvents (a) and concentration dependent emission study of Py-BiimzH_2 in DMSO (b).

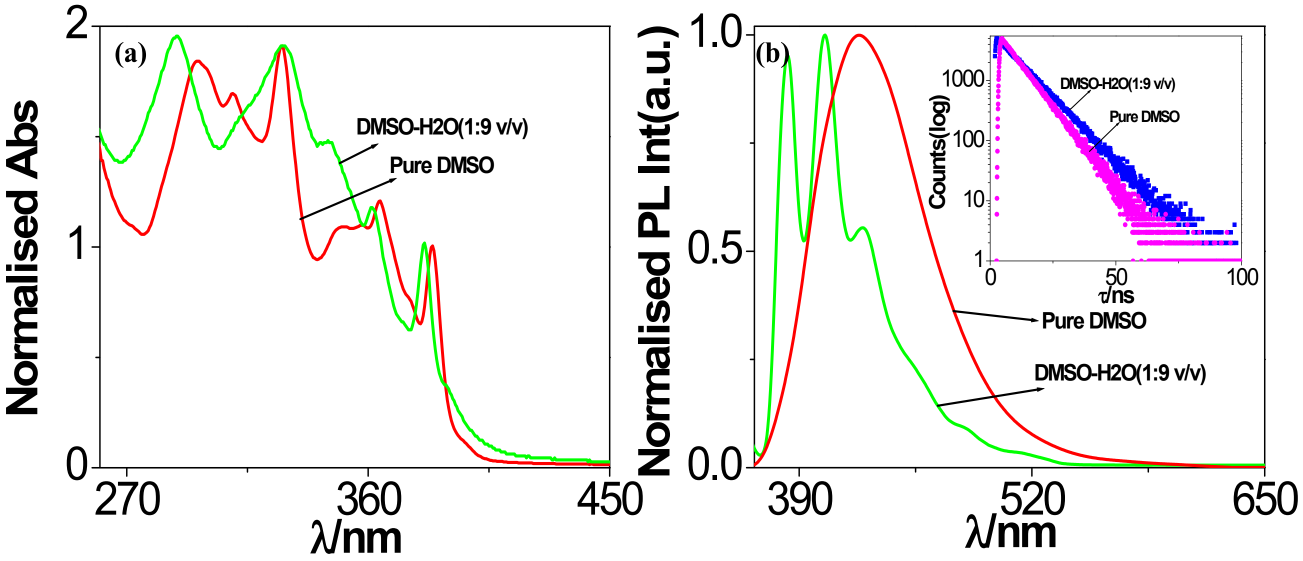

Fig. S8 Normalized UV–vis absorption and luminescence spectrum (λ_{ex}=350 nm) of Py-BiimzH_2 (2.0×10^{-5} M) (a and b, respectively) in DMSO and H_2O-DMSO (9:1 v/v) solution. Inset of (b) shows the lifetime of the receptor.

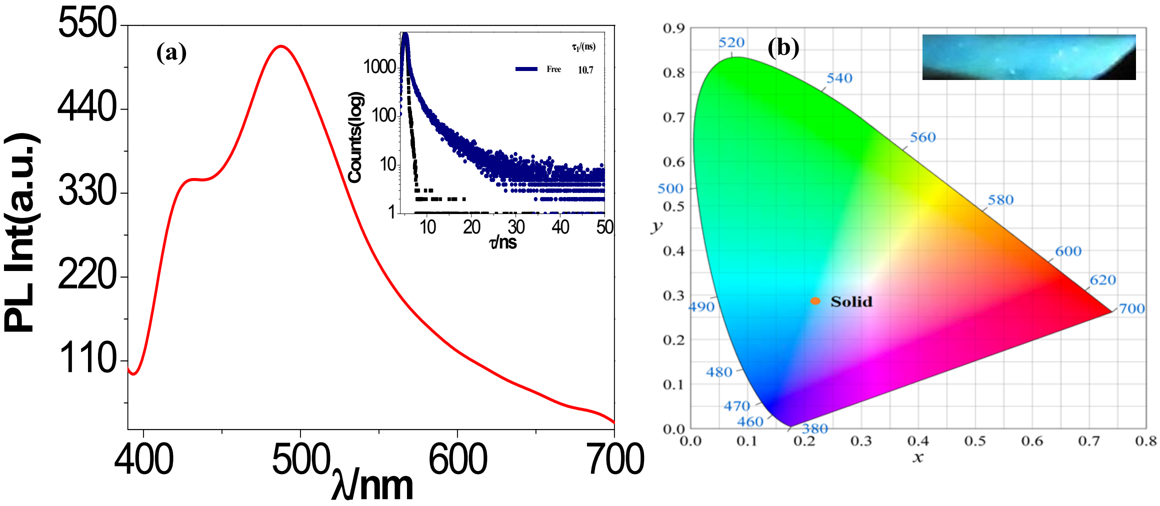

Fig. S9 Emission spectrums of Py-BiimzH$_2$ in solid state (a) with the corresponding CIE coordinate diagram (b). Inset of (a) shows the decay profile while that of (b) shows the fluorescence color in solid state.

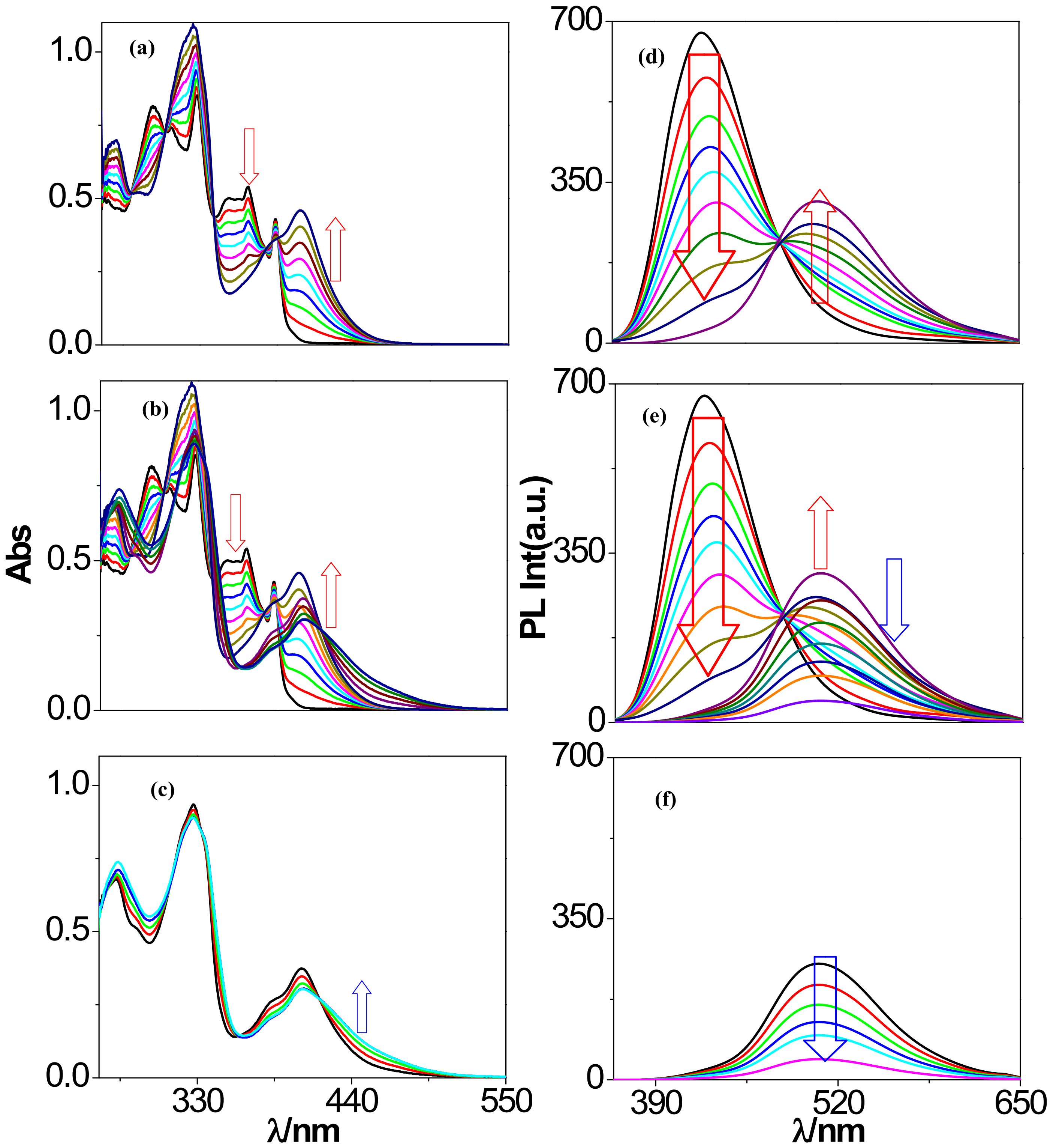

Fig. S10 Changes in UV–vis absorption (a-c) and luminescence (d-f) spectra (λ_{ex}=350 nm) of Py-BiimzH$_2$ (2.0×10^{-5} M) in DMSO upon the addition of OH$^-$ ion (2.0×10^{-2} M).

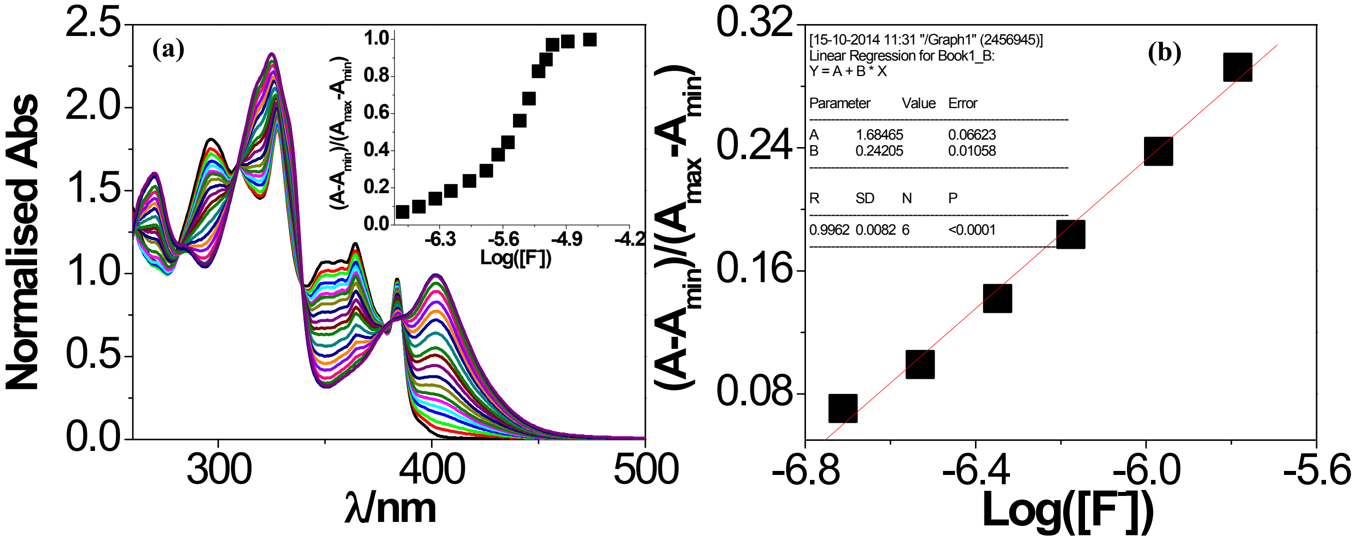

```
[15-10-2014 11:31 "/Graph1" (2456945)]
Linear Regression for Book1_B:
Y = A + B * X

Parameter      Value    Error
------------------------------------------------
A      1.68465     0.06623
B      0.24205     0.01058
------------------------------------------------

R      SD      N      P
------------------------------------------------
0.9962  0.0082  6      <0.0001
------------------------------------------------
```

Fig. S11 (a) Absorption spectral change during the titration of Py-BiimzH_2 (2.0×10^{-5} M) with F^- (2.0×10^{-2} M) in DMSO, inset shows the normalized absorbance between the minimum absorbance (free Py-BiimzH_2) and the maximum absorbance (λ_{abs}=402 nm). (b) A plot of $(A-A_{min})/(A_{max}-A_{min})$ vs Log($[F^-]$), the calculated detection limit of receptor is 1.77×10^{-7} M.

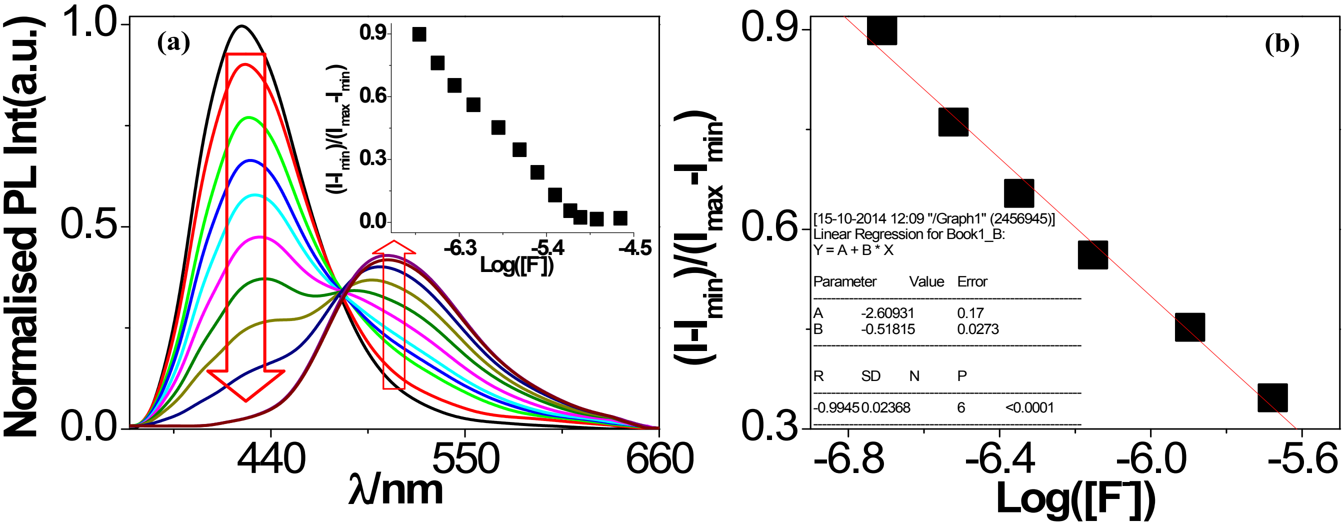

```
[15-10-2014 12:09 "/Graph1" (2456945)]
Linear Regression for Book1_B:
Y = A + B * X

Parameter      Value    Error
------------------------------------------------
A      -2.60931    0.17
B      -0.51815    0.0273
------------------------------------------------

R      SD      N      P
------------------------------------------------
-0.9945 0.02368   6      <0.0001
------------------------------------------------
```

Fig. S12 (a) A fluorescence spectral change during the titration of Py-BiimzH_2 (2.0×10^{-5} M) with F^- (2.0×10^{-2} M) in DMSO, inset shows the normalized intensity between the minimum intensity (free Py-BiimzH_2) and the maximum intensity (λ_{emi}=423 nm). (b) A plot of $(I-I_{min})/(I_{max}-I_{min})$ vs Log($[F^-]$), the calculated detection limit of receptor is 1.54×10^{-7} M.

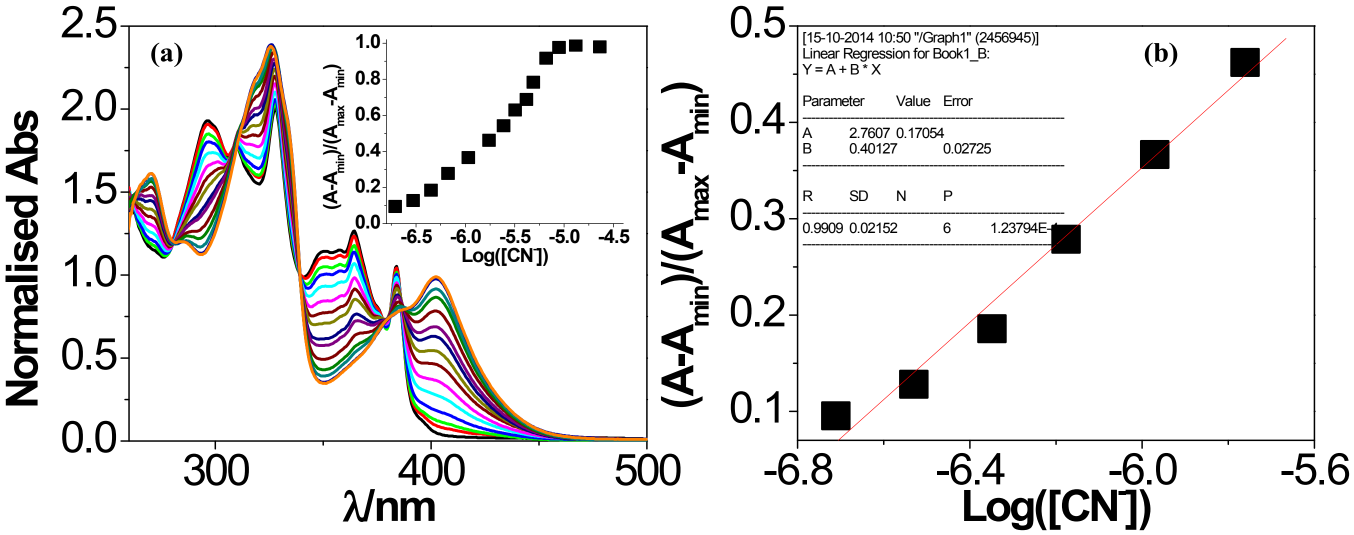

```
[15-10-2014 10:50 "/Graph1" (2456945)]
Linear Regression for Book1_B:
Y = A + B * X

Parameter     Value   Error
------------------------------------------------------------
A        2.7607  0.17054
B        0.40127          0.02725
------------------------------------------------------------

R        SD        N        P
------------------------------------------------------------
0.9909  0.02152            6            1.23794E-
------------------------------------------------------------
```

Fig. S13 (a) Absorption spectral change during the titration of Py-BiimzH$_2$ (2.0×10^{-5} M) with CN$^-$ (2.0 × 10^{-2} M) in DMSO, inset shows the normalized absorbance between the minimum absorbance (free Py-BiimzH$_2$) and the maximum absorbance (λ_{abs}=402 nm). (b) A plot of (A-A$_{min}$)/(A$_{max}$-A$_{min}$) vs Log([CN$^-$]), the calculated detection limit of receptor is 1.98 × 10^{-7} M.

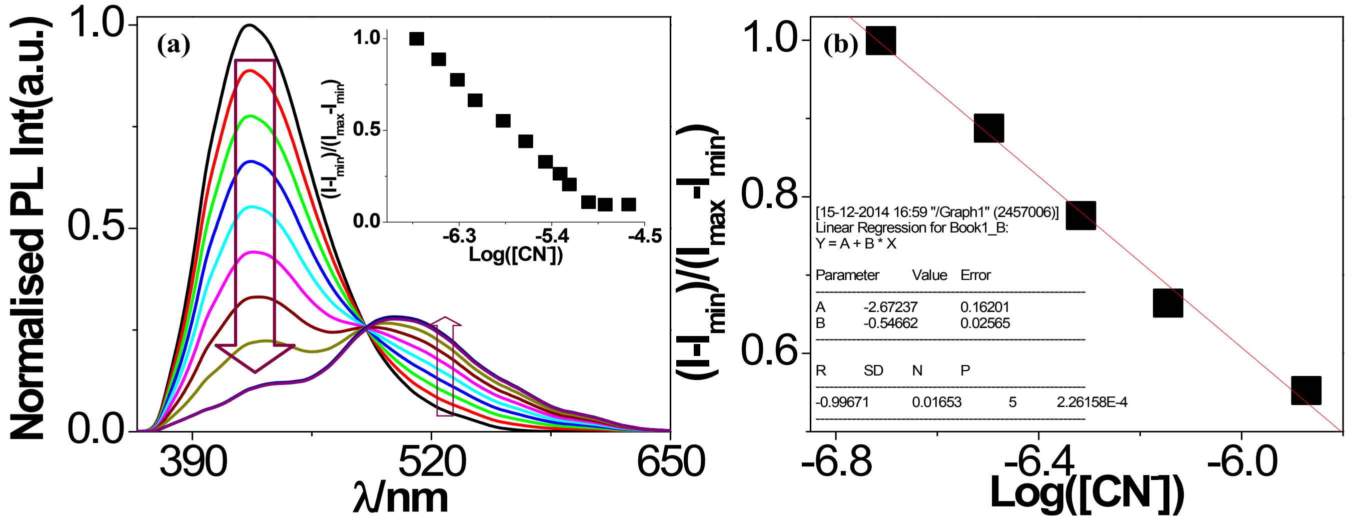

```
[15-12-2014 16:59 "/Graph1" (2457006)]
Linear Regression for Book1_B:
Y = A + B * X

Parameter     Value    Error
------------------------------------------------------------
A        -2.67237      0.16201
B        -0.54662      0.02565
------------------------------------------------------------

R        SD        N        P
------------------------------------------------------------
-0.99671        0.01653          5        2.26158E-4
------------------------------------------------------------
```

Fig. S14 (a) A fluorescence spectral change during the titration of Py-BiimzH$_2$ (2.0×10^{-5} M) with CN$^-$ (2.0 × 10^{-2} M) in DMSO, inset shows the normalized intensity between the minimum intensity (free Py-BiimzH$_2$) and the maximum intensity (λ_{emi}=423 nm). (b) A plot of (I-I$_{min}$)/(I$_{max}$-I$_{min}$) vs Log([CN$^-$]), the calculated detection limit of receptor is 1.70 × 10^{-7} M.

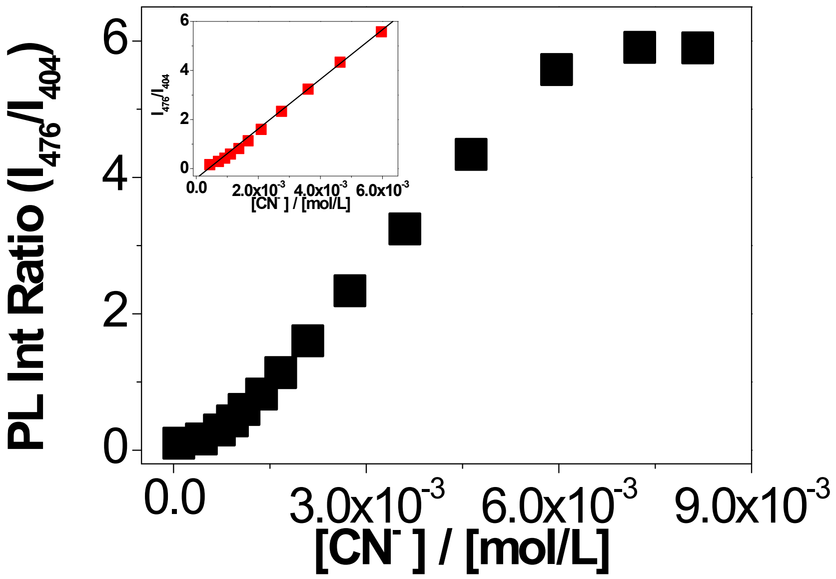

Fig. S15 Fluorescence intensity ratio plot (I_{476nm}/I_{404nm}) of Py-BiimzH$_2$ (2.0 × 10^{-5} M) as a function of CN$^-$ concentration in 1:9 DMSO-H$_2$O media. Inset shows the linear dependence of the intensity ratio plot with CN$^-$.

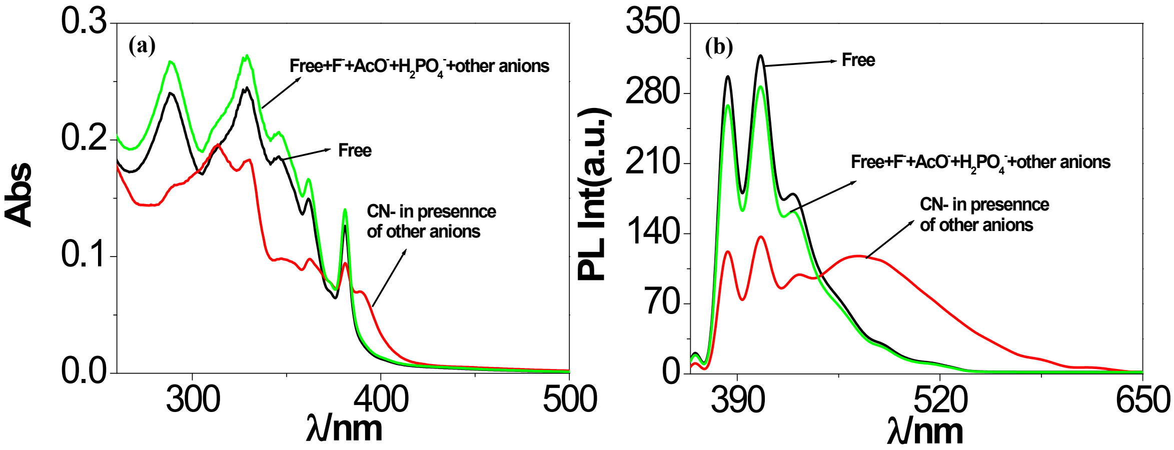

Fig. S16 Changes in UV-vis absorption (a) and luminescence (b) spectra (λ_{ex}=350 nm) of Py-BiimzH$_2$ (2.0×10^{-5} M) in DMSO and H$_2$O-DMSO (9:1 v/v) upon the addition of 300 equiv of CN$^-$ in presence of other anions.

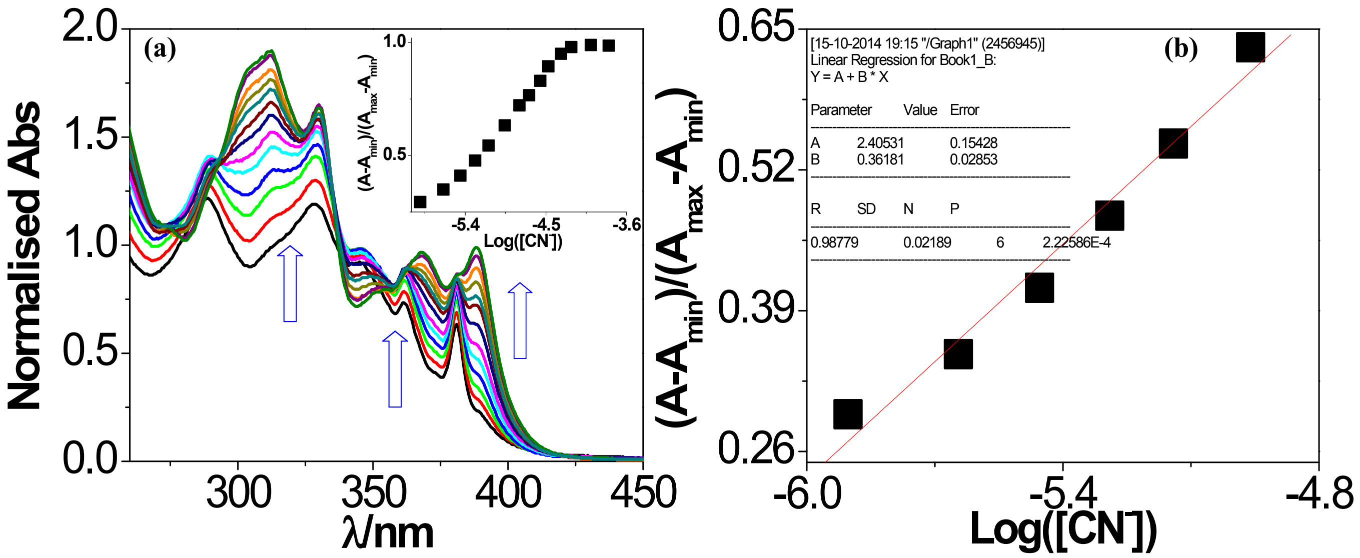

Fig. S17 (a) Absorption spectral change during the titration of Py-BiimzH$_2$ (2.0×10^{-5} M) with CN$^-$ (1.5×10^{-1} M) in H$_2$O-DMSO (9:1 v/v) solution, inset shows the normalized absorbance between the minimum absorbance (free Py-BiimzH$_2$) and the maximum absorbance (λ_{abs}=388 nm). (b) A plot of (A-A$_{min}$)/(A$_{max}$-A$_{min}$) vs Log([CN$^-$]), the calculated detection limit of receptor is 1.10×10^{-6} M.

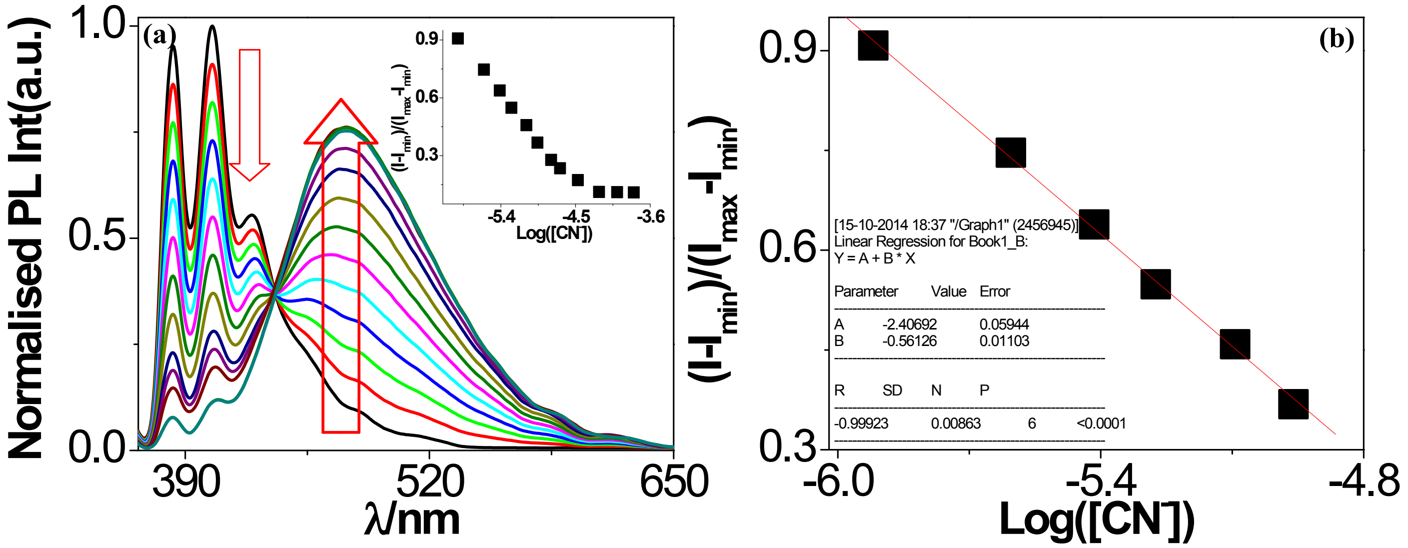

Fig. S18 (a) A fluorescence spectral change during the titration of Py-BiimzH$_2$ (2.0×10^{-5} M) with CN$^-$ (1.5×10^{-1} M) in H$_2$O-DMSO (9:1 v/v) solution, inset shows the normalized intensity between the minimum intensity (free Py-BiimzH$_2$) and the maximum intensity (λ_{emi}=404 nm). (b) A plot of (I-I$_{min}$)/(I$_{max}$-I$_{min}$) vs Log([CN$^-$]), the calculated detection limit of receptor is 1.04×10^{-6} M.

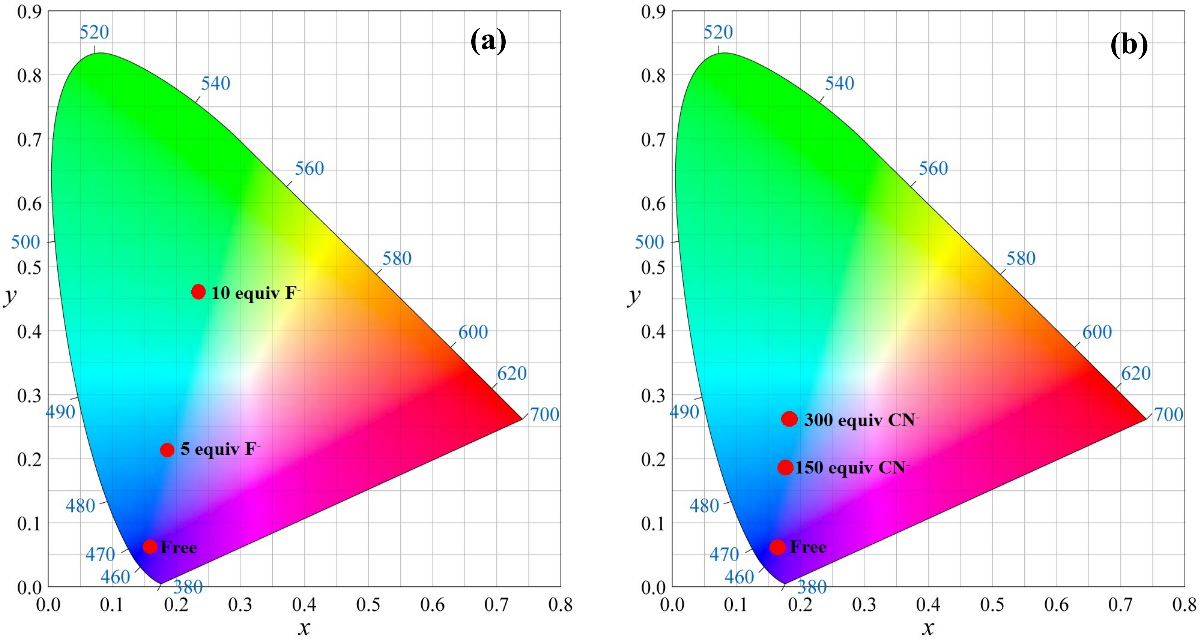

Fig. S19 Chromaticity diagram of Py-BiimzH$_2$ (2.0×10^{-5} M) with increasing amount of F$^-$ (2.0×10^{-2} M) in DMSO (a) and CN$^-$ (1.5×10^{-1} M) in H$_2$O-DMSO (9:1 v/v) solution (b).

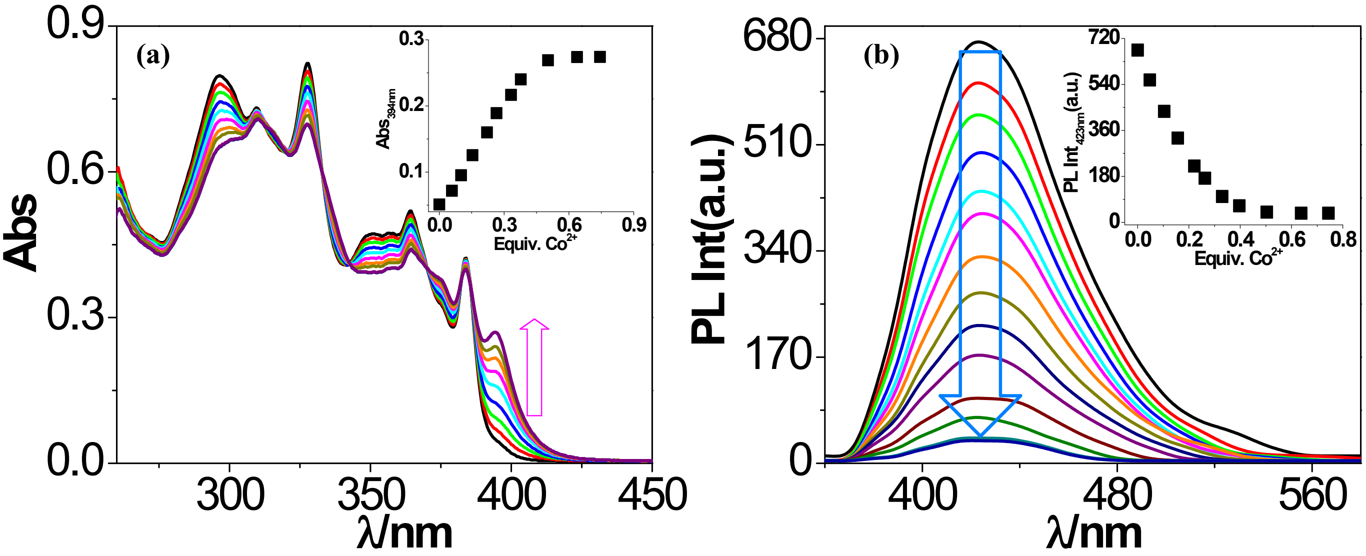

Fig. S20 Changes in UV-vis absorption and photoluminescence spectra (λ_{ex}=350 nm) (a and b respectively) of Py-BiimzH_2 (2.0×10^{-5} M) in DMSO upon addition of $Co(ClO_4)_2$ (5.0×10^{-3} M). The insets show the change of absorption (λ_{abs}=394 nm) and emission (λ_{emi}=423 nm) intensity as a function of the equivalent of Co^{2+} ion added.

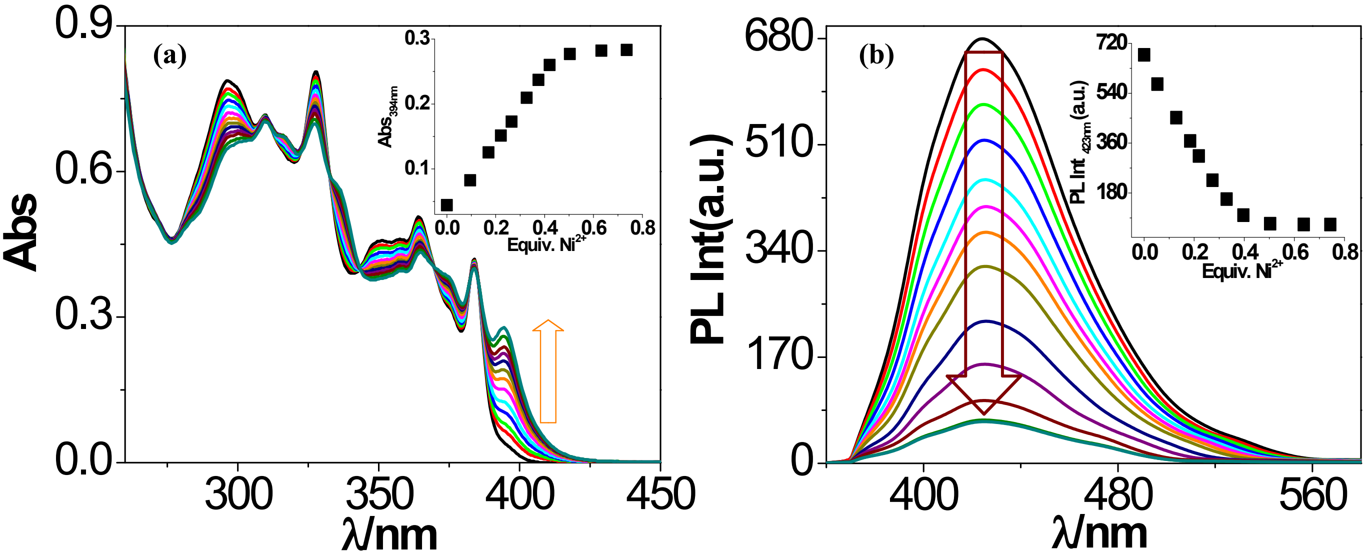

Fig. S21 Changes in UV-vis absorption and photoluminescence spectra (λ_{ex}=350 nm) (a and b respectively) of Py-BiimzH_2 (2.0×10^{-5} M) in DMSO upon addition of $Ni(ClO_4)_2$ (5.0×10^{-3} M). The insets show the change of absorption (λ_{abs}=394 nm) and emission (λ_{emi}=423 nm) intensity as a function of the equivalent of Ni^{2+} ion added.

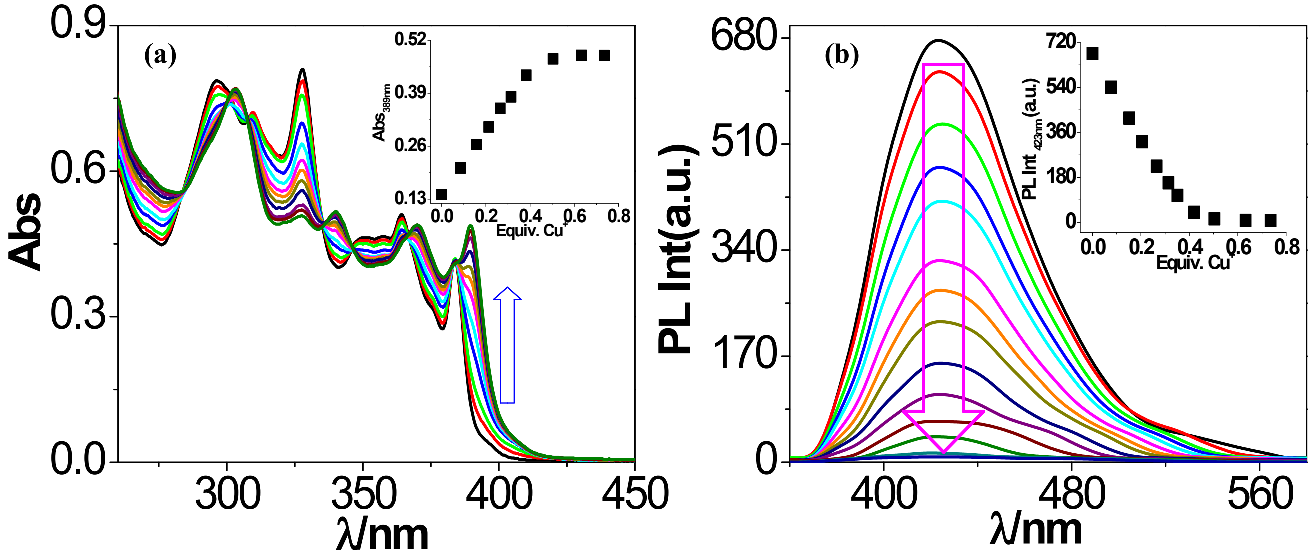

Fig. S22 Changes in UV-vis absorption and photoluminescence spectra (λ_{ex}=350 nm) (a and b respectively) of Py-BiimzH$_2$ (2.0×10^{-5} M) in DMSO upon addition of Cu(ClO$_4$) (5.0 × 10^{-3} M). The insets show the change of absorption (λ_{abs}=389 nm) and emission (λ_{emi}=423 nm) intensity as a function of the equivalent of Cu$^+$ ion added.

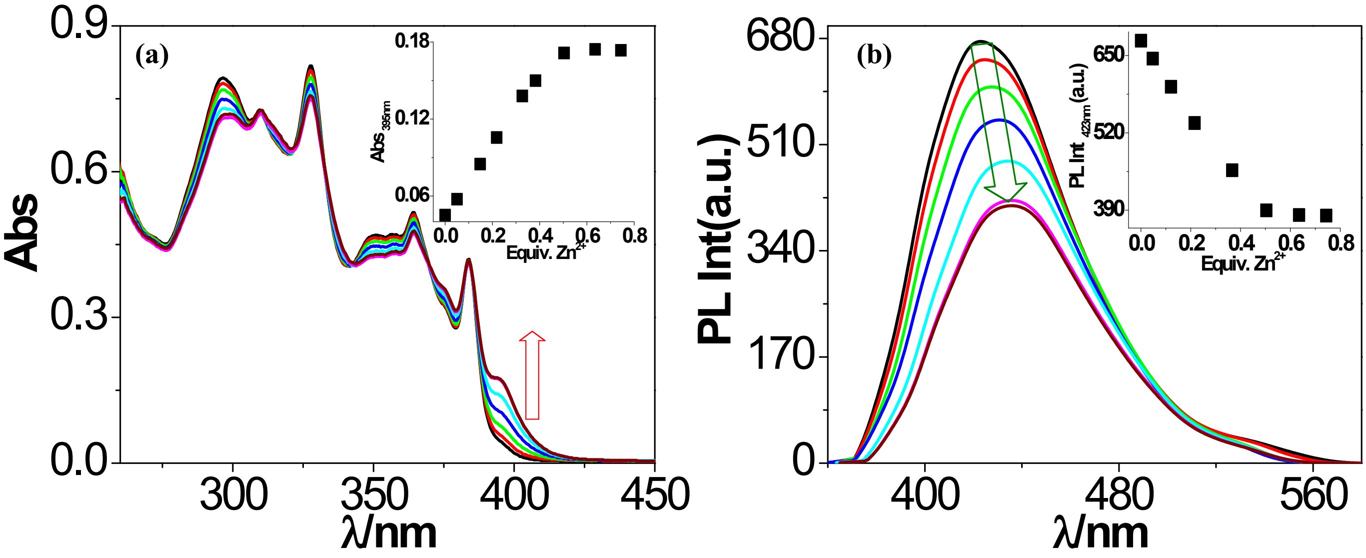

Fig. S23 Changes in UV-vis absorption and photoluminescence spectra (λ_{ex}=350 nm) (a and b respectively) of Py-BiimzH$_2$ (2.0×10^{-5} M) in DMSO upon addition of Zn(ClO$_4$)$_2$ (5.0 × 10^{-3} M). The insets show the change of absorption (λ_{abs}=395 nm) and emission (λ_{emi}=423 nm) intensity as a function of the equivalent of Zn^{2+} ion added.

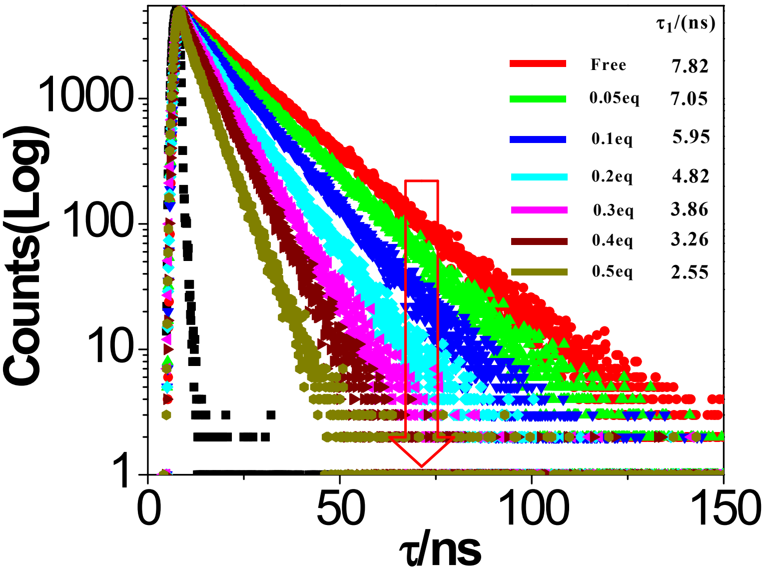

Fig. S24 Changes in excited-state decay profiles of Py-BiimzH$_2$ (2.0×10^{-5} M) in DMSO upon incremental addition of Cu^{2+} ion (5.0 × 10^{-3} M). Lifetimes values are also given in the inset of the figure.

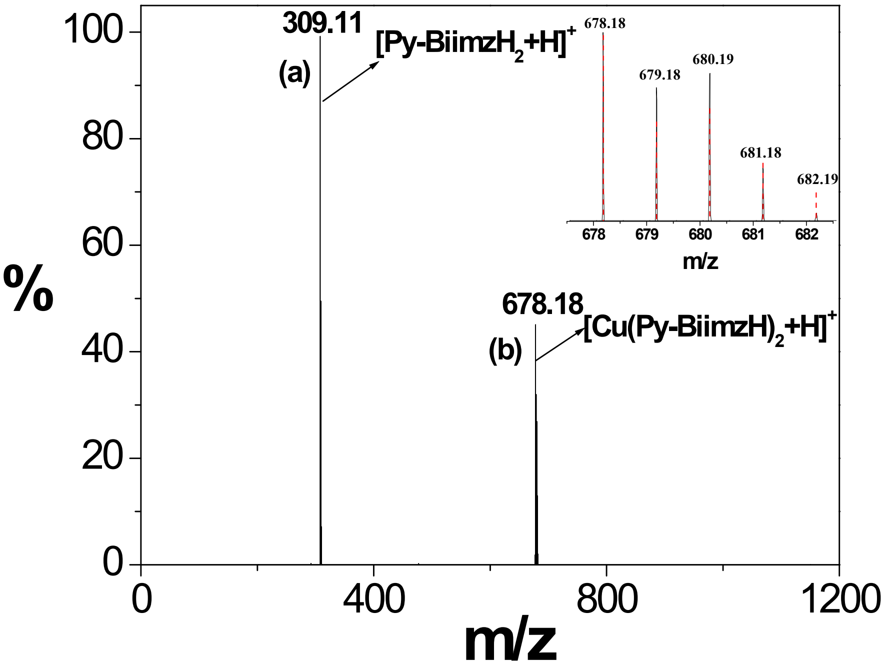

Fig. S25 ESI-MS (positive) for the free receptor Py-BiimzH$_2$ (a) (*m/z* = 308.11) and the complex cation [Cu(Py-BiimzH)$_2$+H]$^+$ (b) (*m/z* = 678.18) in DMSO showing the observed and isotopic distribution patterns.

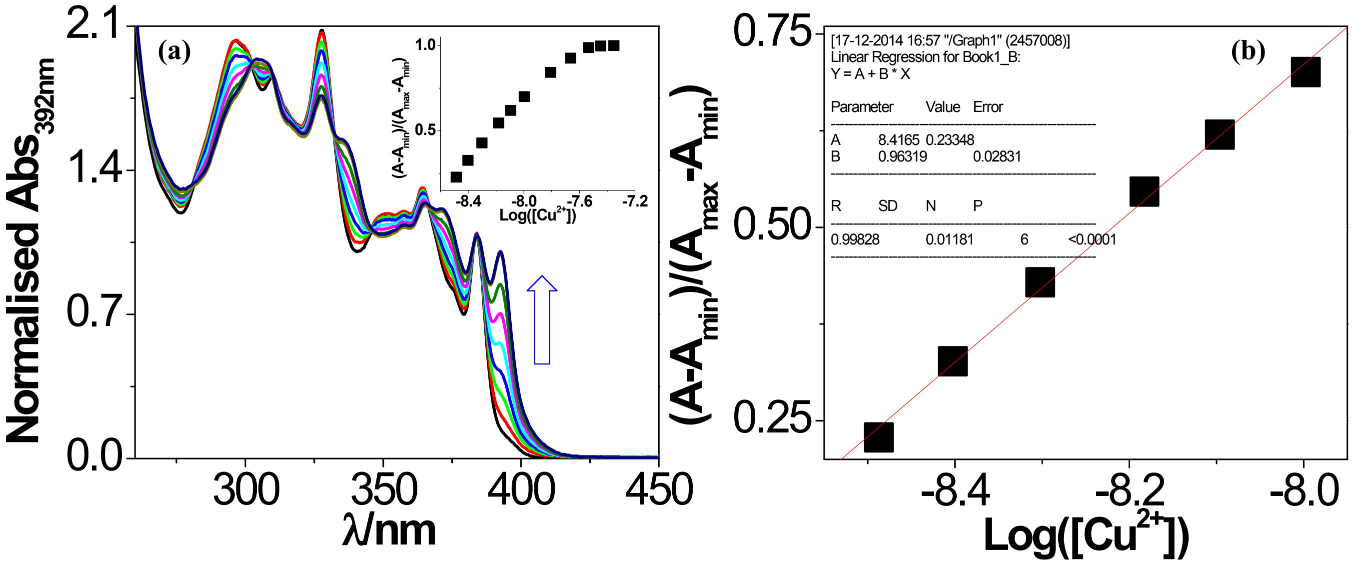

Fig. S26 (a) Absorption spectral change during the titration of Py-BiimzH$_2$ (2.0×10^{-5} M) with Cu^{2+} (5.0×10^{-3} M) in DMSO solution, inset shows the normalized absorbance between the minimum absorbance (free Py-BiimzH$_2$) and the maximum absorbance (λ_{abs}=392 nm). (b) A plot of $(A-A_{min})/(A_{max}-A_{min})$ vs Log([Cu^{2+}]), the calculated detection limit of receptor is 2.95 $\times 10^{-9}$ M.

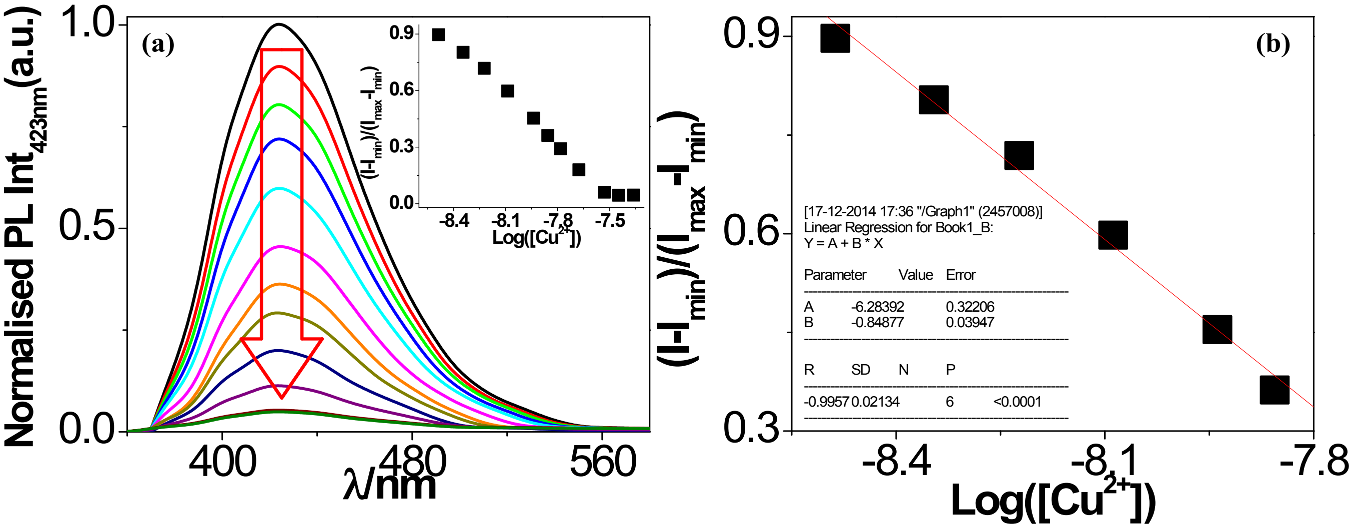

Fig. S27 (a) A fluorescence spectral change during the titration of Py-BiimzH$_2$ (2.0×10^{-5} M) with Cu^{2+} (5.0×10^{-3} M) in DMSO, inset shows the normalized intensity between the minimum intensity (free Py-BiimzH$_2$) and the maximum intensity (λ_{emi}=423 nm). (b) A plot of $(I-I_{min})/(I_{max}-I_{min})$ vs Log([Cu^{2+}]), the calculated detection limit of receptor is 3.17 $\times 10^{-9}$ M.

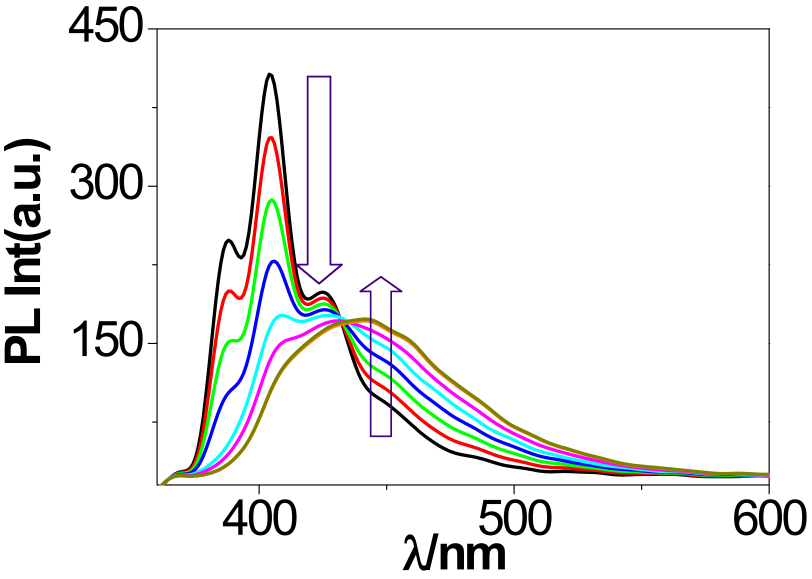

Fig. S28 Changes in the luminescence spectra of Py-BiimzH_2 (2.0×10^{-5} M) with incremental addition of Zn^{2+} ion (up to 0.5 equiv) in 1:1 DMSO-MeOH solution.

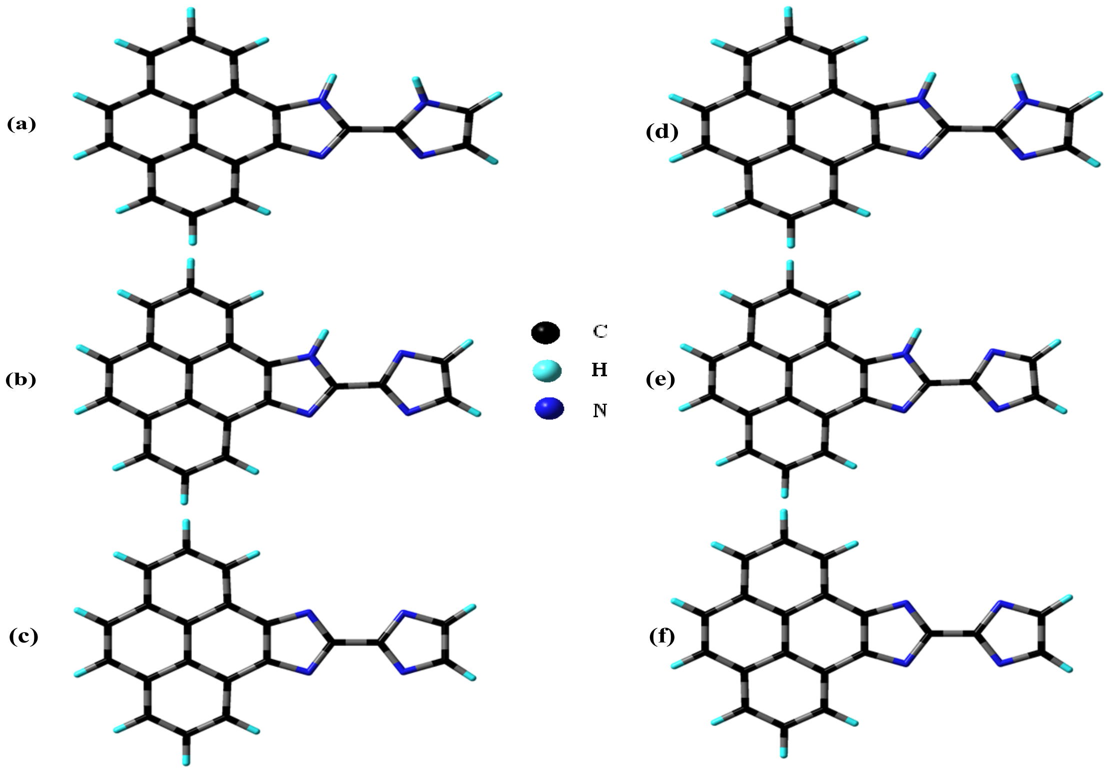

Fig. S29 Ground state (a-c) and singlet excited state (d-f) optimized geometries of Py-BiimzH$_2$, Py-BiimzH and Py-Biimz in DMSO, respectively.

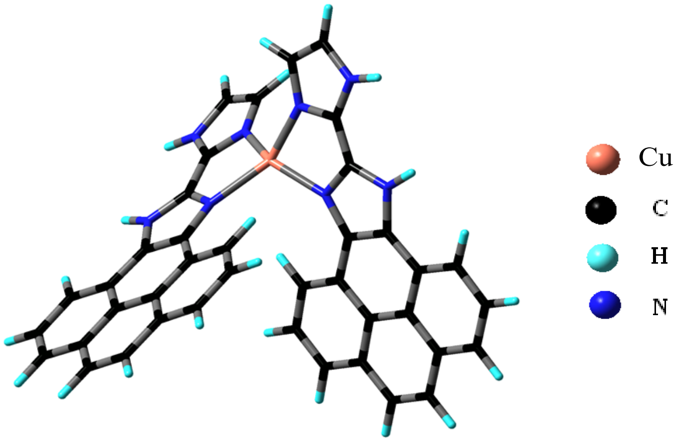

Fig. S30 Ground state optimized geometry of [Cu(Py-BiimzH$_2$)$_2$]$^{2+}$ in DMSO.

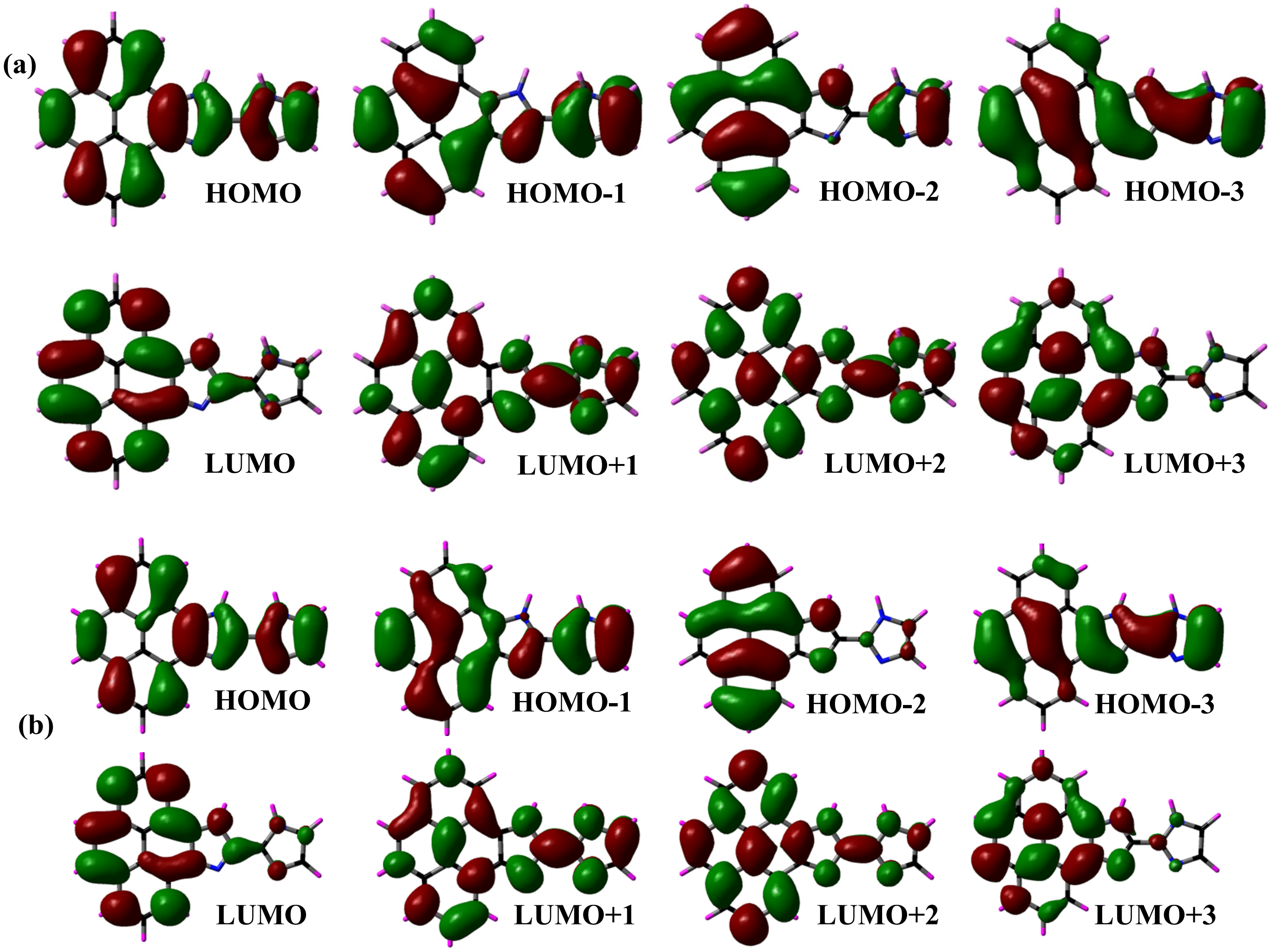

Fig. S31 Schematic drawings of the selective frontier molecular orbitals of **Py**-BiimzH_2 in the ground (a) and singlet excited state (b) in DMSO.

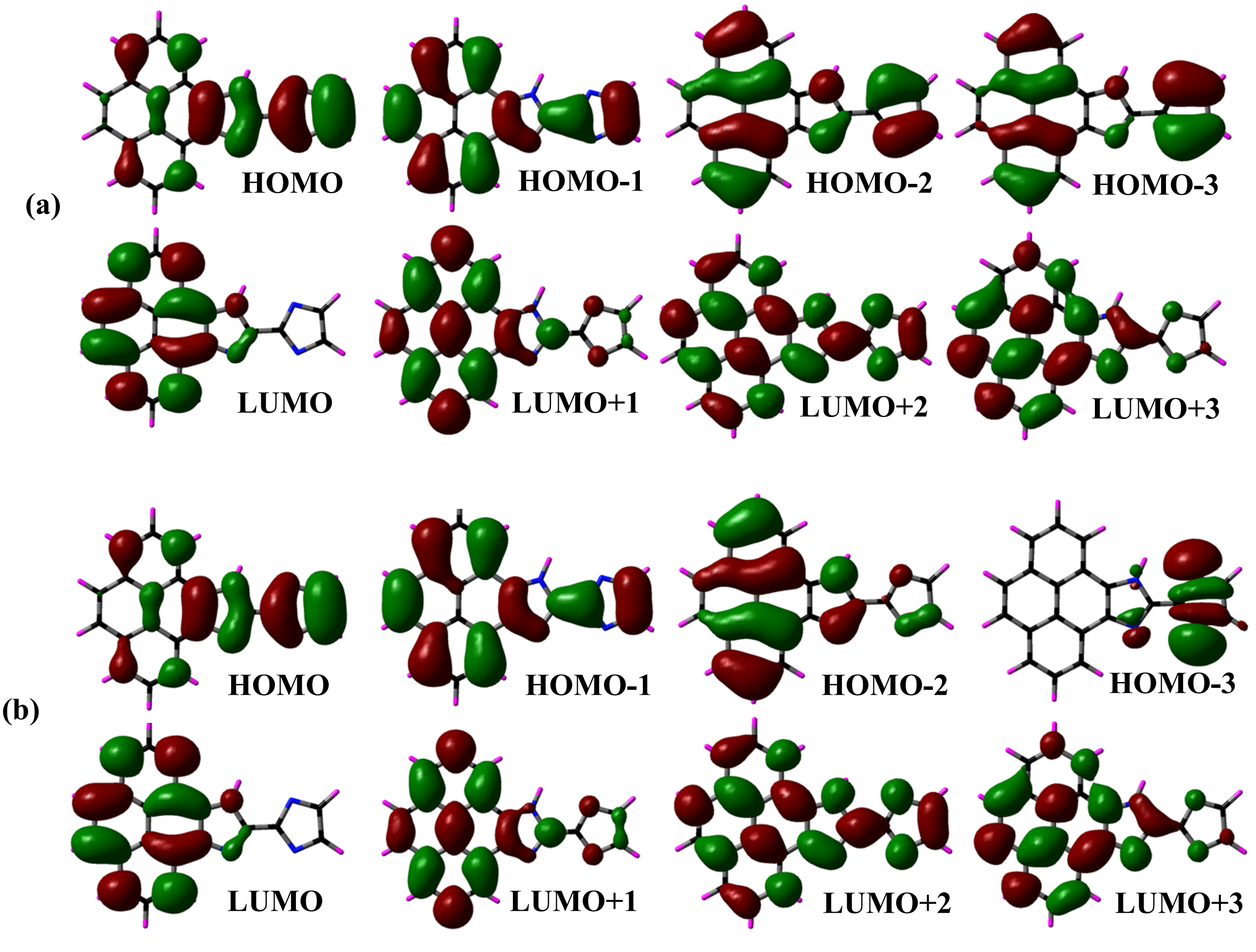

Fig. S32 Schematic drawings of the selective frontier molecular orbitals of Py-BiimzH in the ground (a) and singlet excited state (b) in DMSO.

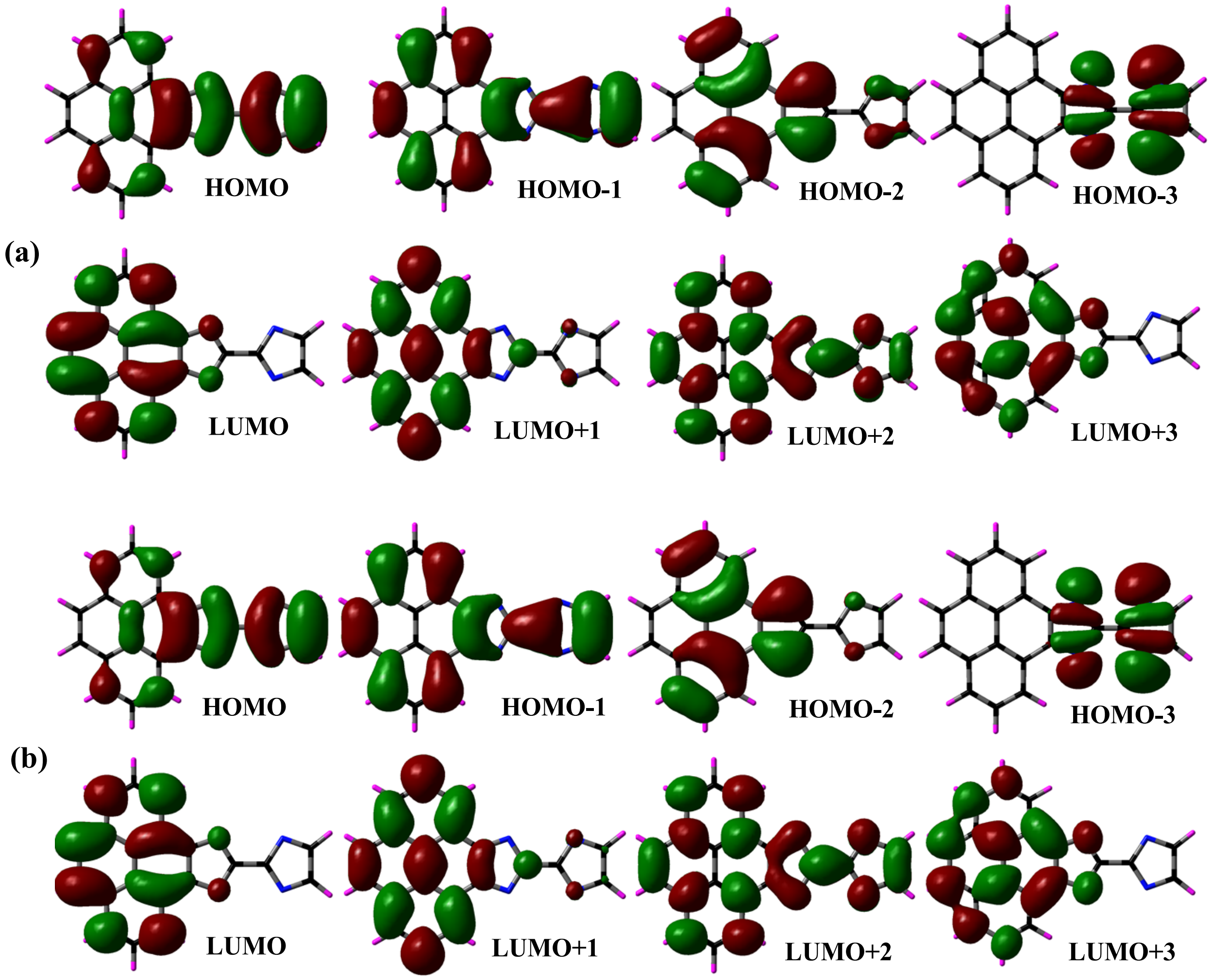

Fig. S33 Schematic drawings of the selective frontier molecular orbitals of Py-Biimz in the ground (a) and singlet excited state (b) in DMSO.

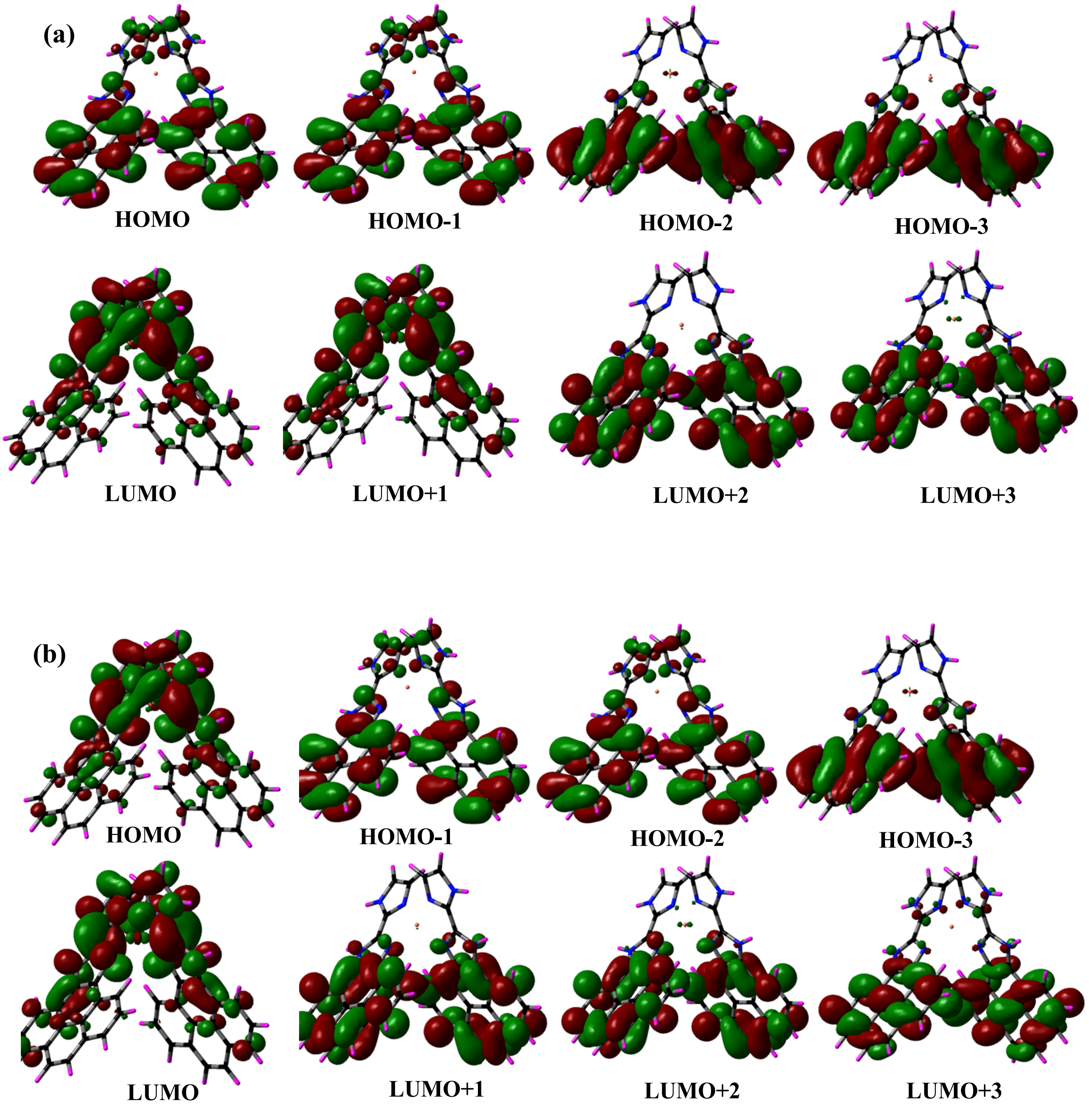

Fig. S34 Schematic drawings of the selective frontier molecular orbitals of [Cu(Py-BiimzH$_2$)$_2$]$^{2+}$ in α spin (a) and β spin (b) sate in the ground state in DMSO.

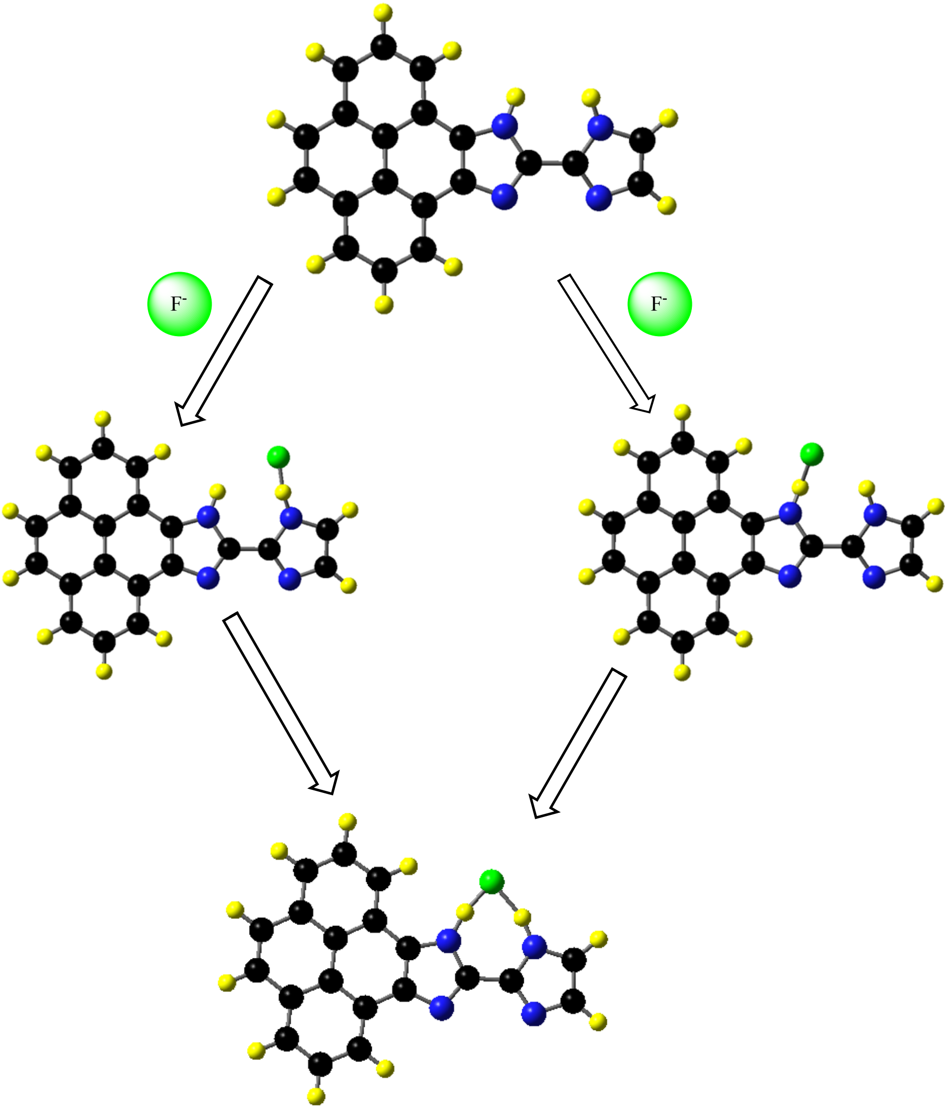

Fig. S35 Optimised structure obtained for Py-BiimzH$_2$ with 1 equiv of F$^-$ ion in DMSO solution.

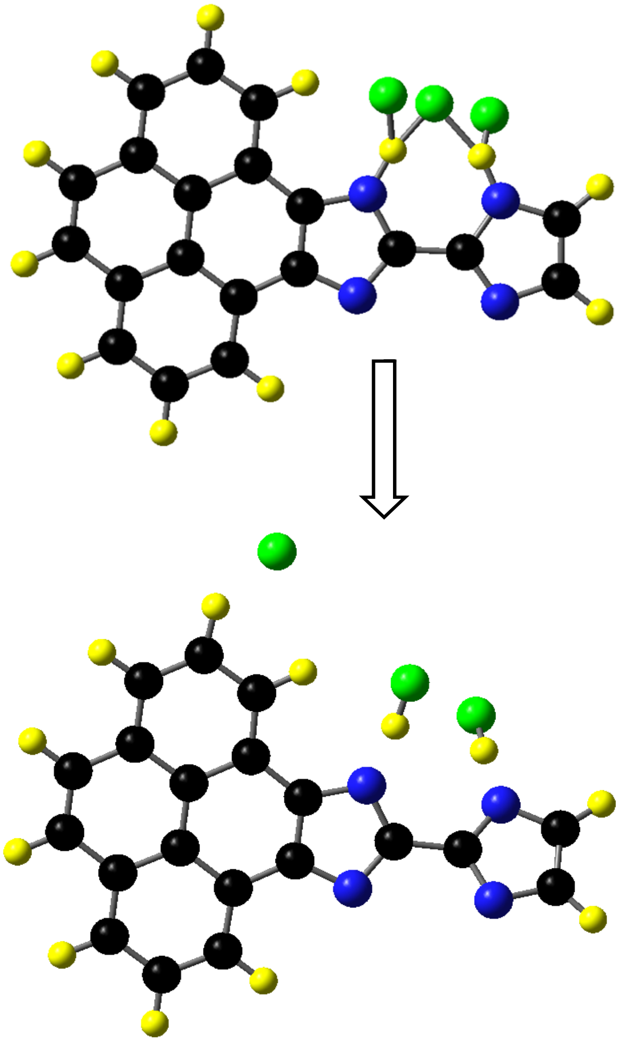

Fig. S36 Optimised structure obtained for Py-BiimzH_2 with excess of F^- ion in DMSO solution.

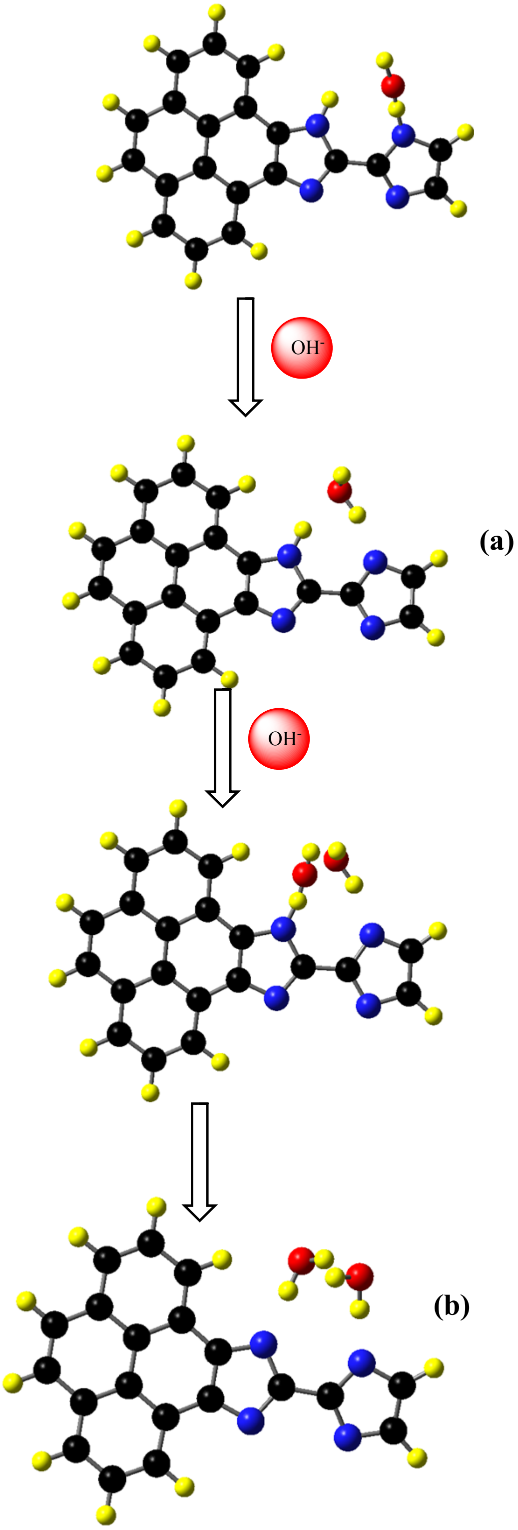

Fig. S37 Optimised structure obtained for Py-BiimzH$_2$ with 1 equiv (a) and excess (b) of OH$^-$ ion in DMSO solution.

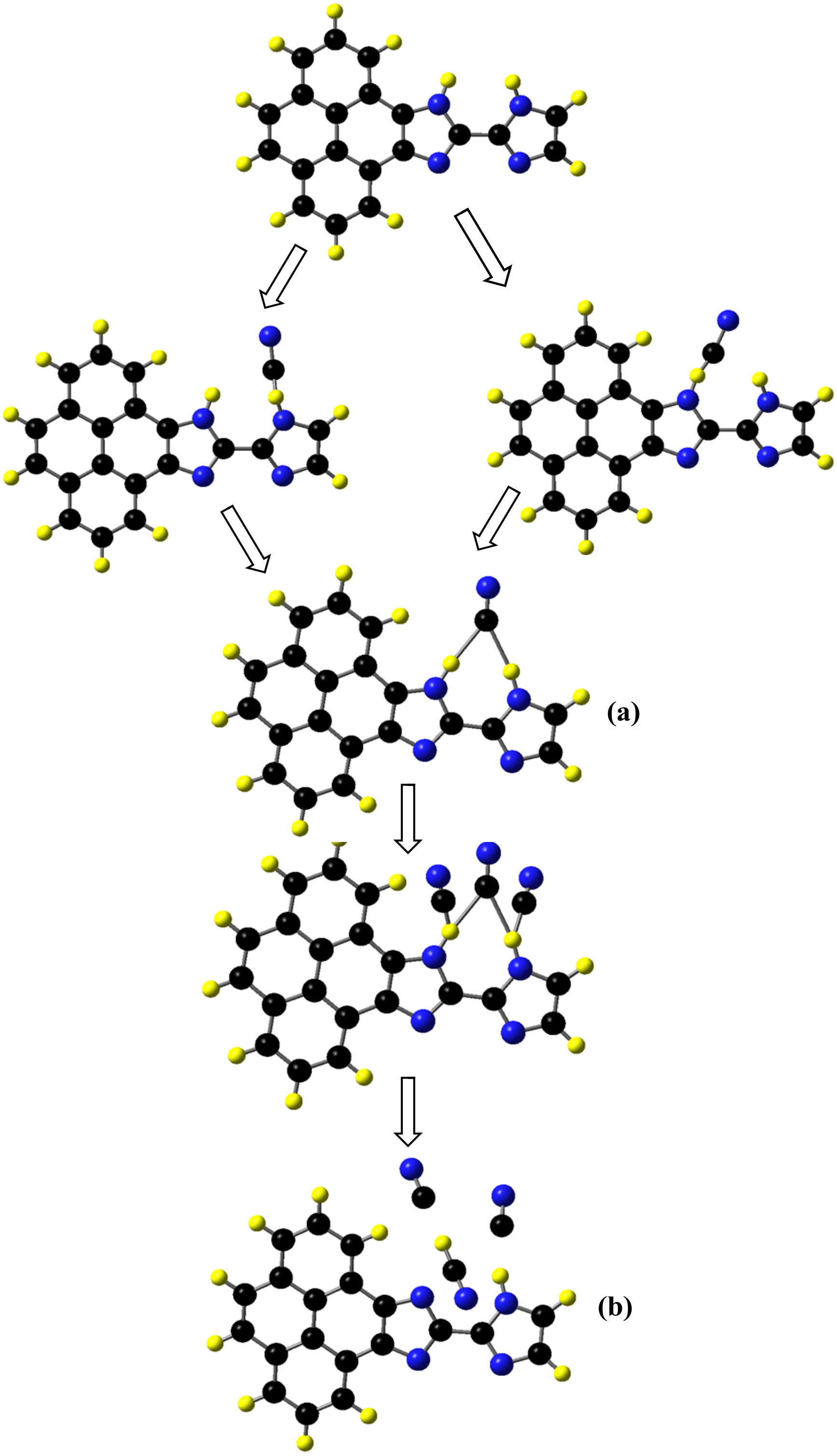

Fig. S38 Optimised structure obtained for Py-BiimzH_2 with 1 equiv (a) and excess (b) of CN^- ion in water solution.

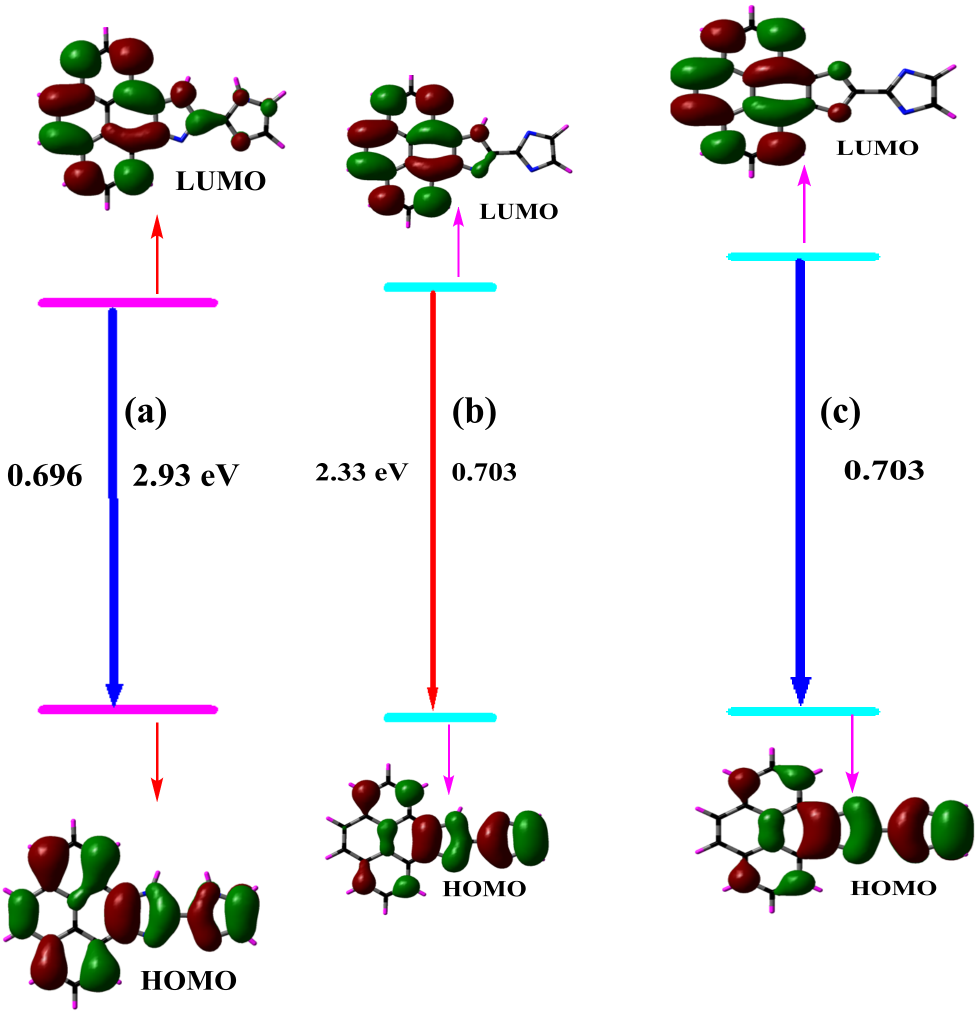

Fig. S39 Calculated single electron transition for the emission from S_1 state of Py-BiimzH_2 (a), Py-BiimzH (b), and Py-Biimz (c) respectively**,** in DMSO.

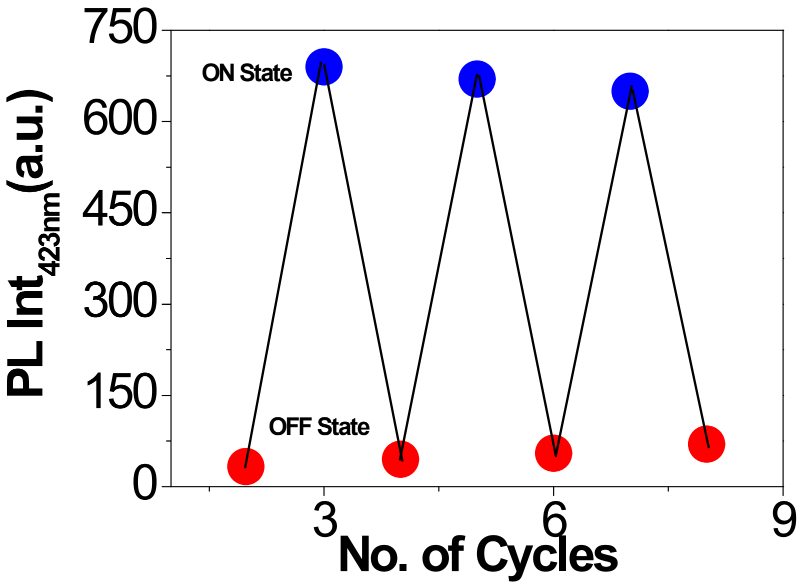

Fig. S40 Changes in the luminescence intensity of Py-BiimzH$_2$ (2.0× 10^{-5} M) at 423nm upon coordination with Cu^{2+} followed by its de-coordination with CN$^-$ (many cycles).

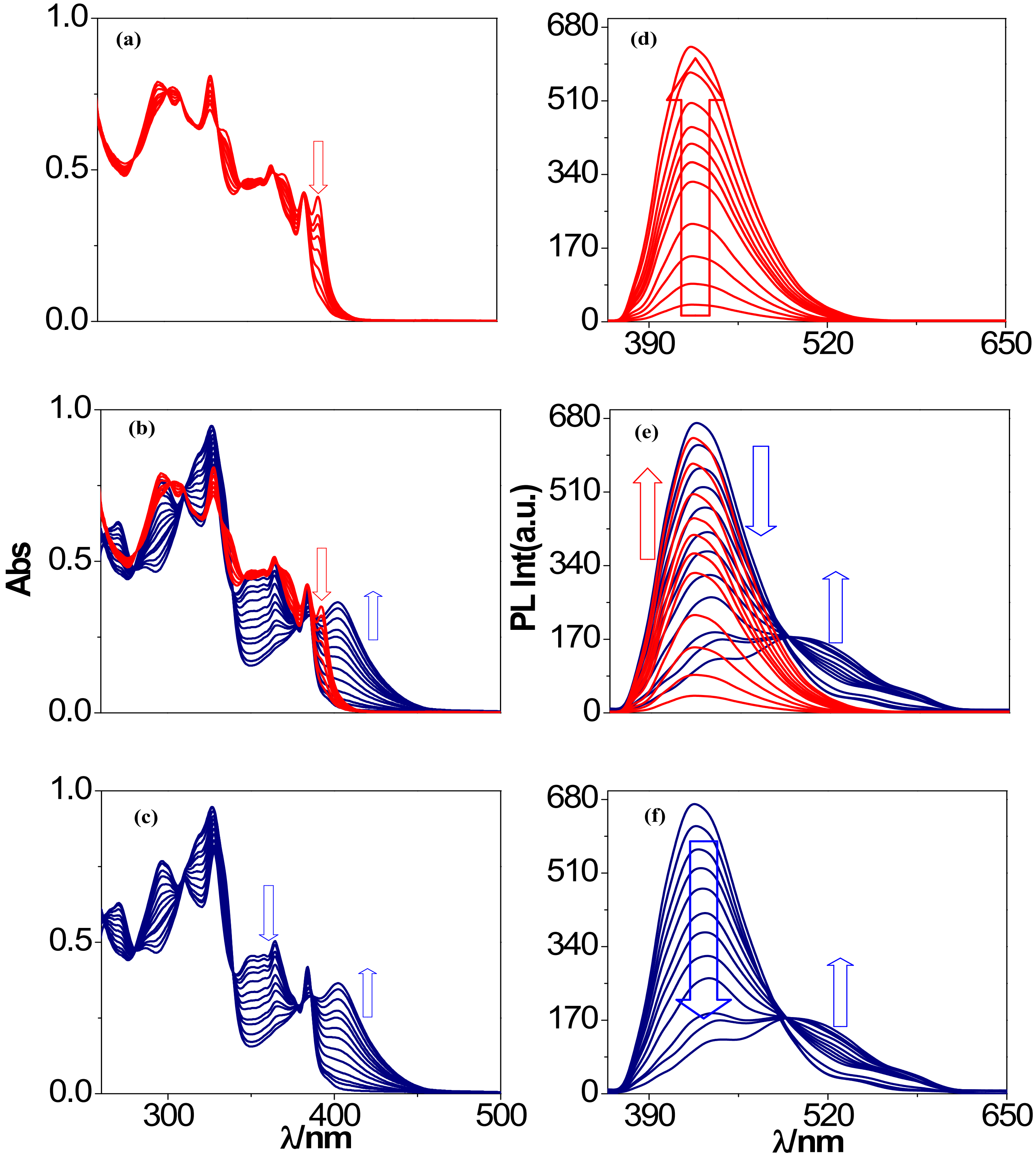

Fig. S41 Changes in UV-vis (a-c) and photoluminescence (d-f) spectra of $[Cu(Py\text{-}BiimzH_2)_2]^{2+}$ in DMSO upon incremental addition of CN^- ion.

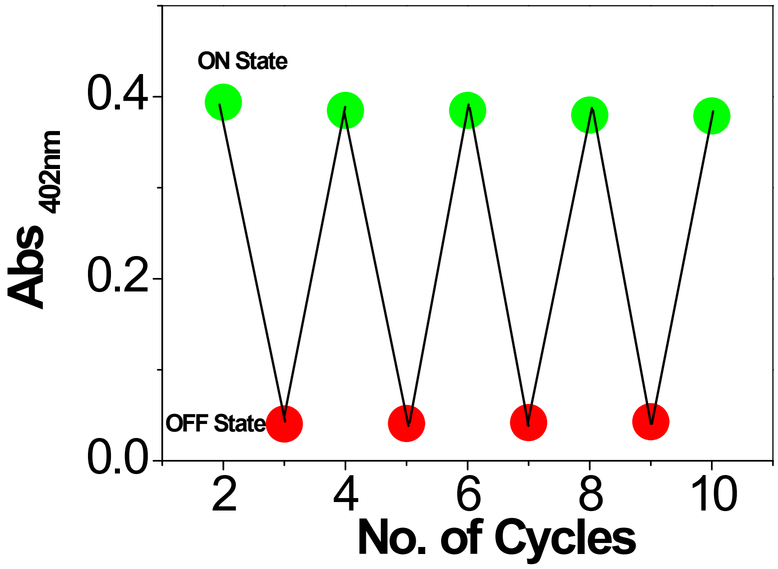

Fig. S42 Changes in absorbance of Py-BiimzH$_2$ (2.0 × 10^{-5} M) at 402 nm upon deprotonation with CN$^-$ followed by reversible protonation with H$^+$ (many cycles).

Reference:

[S1] Schneider, H.-J.; Yatsimirsky, A. *Principles and Methods in Supramolecular Chemistry*; John Wiley & Sons: England, 2000, 142.

[S2] SAINT (version 6.02), SADABS (version 2.03); Bruker AXS Inc.: Madison, WI, 2002.

[S3] SHELXTL, (version 6.10); Bruker AXS Inc.: Madison, WI, 2002.

[S4] Sheldrick, G. M. SHELXL-97, *Program for the Refinement of crystal Structures*; University of Göttingen: Göttingen, Germany, 1997.

[S5] PLATON; Spek, A. L. *J. Appl. Cryst.* 2003, **36,** 7-13.

[S6] M. J. Frisch, G. W. Trucks, H. B. Schlegel, G. E. Scuseria, M. A. Robb, J. R. Cheeseman, G. Scalmani, V. Barone, B. Mennucci, G. A. Petersson, H. Nakatsuji, M. Caricato, X. Li, H. P. Hratchian, A. F. Izmaylov, J. Bloino, G. Zheng, J. L. Sonnenberg, M. Hada, M. Ehara, K. Toyota, R. Fukuda, J. Hasegawa, M. Ishida, T. Nakajima, Y. Honda, O. Kitao, H. Nakai, T. Vreven, J. A. Montgomery, J. E.Jr.; Peralta, F. Ogliaro, M. Bearpark, J. J. Heyd, E. Brothers, K. N. Kudin, V. N.Staroverov, R. Kobayashi, J. Normand, K. Raghavachari, A. Rendell, J. C. Burant, S. S. Iyengar, J. Tomasi, M. Cossi, N. Rega, J. M. Millam, M. Klene, J. E. Knox, J. B. Cross, V. Bakken, C. Adamo, J. Jaramillo, R. Gomperts, R. E. Stratmann, O. Yazyev, A. J. Austin, R. Cammi, C. Pomelli, J. W. Ochterski, R. L. Martin, K. Morokuma, V. G. Zakrzewski, G. A. Voth, P. Salvador, J. J. Dannenberg, S. Dapprich, A. D. Daniels, Ö. Farkas, J. B. Foresman, J. V. Ortiz, J. Cioslowski and D. J. Fox, Gaussian 09, revision A.02; Gaussian Inc.: Wallingford, CT, 2009.

[S7] A. D. Becke, *J. Chem. Phys.*, 1993**, 98**, 5648-5652.

[S8] C. T. Lee, W. T. Yang and R. G. Parr, *Phys. Rev. B*, 1988, **37**, 785-789.

[S9] M. E. Casida, C. Jamorski, K. C. Casida and D. R. Salahub, *J. Chem. Phys.* 1998, **108**, 4439-4449.

[S10] R. E. Stratmann, G. E. Scuseria and M. J. Frisch, *J. Chem. Phys.,* 1998, **109**, 8 218-8224.

[S11] M. Caricato, B. Mennucci, J. Tomasi, F. Ingrosso, R. Cammi, S. Corni and G. Scalmani, , *J. Chem. Phys* ., 2006, **124**, 124520.

[S12] B. Mennucci, C. Cappelli, C. A. Guido, R. Cammi and J. Tomasi, *J. Phy. Chem. A*, 2009, **113**, 3009-3020.

[S13] R. II. Dennington, T. Keith and J. Millam, Gauss View 3; Semichem, Inc.: Shawnee Mission, KS, 2007.

[S14] N. M. O Boyle, A. L. Tenderholt and K. M. Langner, *J. of Comput. Chem*. 2008**, 29**, 839-845.